Advances in Applied Mathematics and Mechanics
Adv. Appl. Math. Mech., Vol. **18**, No. 1, pp. 11-36

DOI: 10.4208/aamm.OA-2024-0069
February 2026

Adaptive Finite Element Method for Simulating Graphene Surface Plasmon Resonance

Jingrun Chen[1,2], Xuhong Liu[1], Jiangqiong Mao[3] and Wei Yang[3,*]

[1] *School of Mathematical Sciences, University of Science and Technology of China, Hefei, Anhui 230026, China*
[2] *Suzhou Institute for Advanced Research, University of Science and Technology of China, Suzhou, Jiangsu 215123, China*
[3] *Hunan Key Laboratory for Computation and Simulation in Science and Engineering, School of Mathematics and Computational Science, Xiangtan University, Xiangtan, Hunan 411105, China*

Received 4 April 2024; Accepted (in revised version) 13 August 2024

Abstract. In this paper, we present the design of a posteriori error estimator for the plasmon phenomenon on the graphene surface and propose a method to achieve local high-precision numerical calculations when plasmon phenomena occur on the graphene surface. We provide a lower bound estimate for the posteriori error estimator, along with a proof of convergence. Specifically, the constructed posterior error estimator enables local refinement in regions where the error is significant at the graphene interface. Firstly, we outline the construction of the posterior error estimator and provide the proof of its lower bound. Secondly, we establish the convergence of the Adaptive Edge Finite Element Method (AEFEM). Finally, we present numerical results that validate the effectiveness of the error estimator.

AMS subject classifications: 35R30, 65N30

Key words: Surface plasmon phenomenon, time-harmonic Maxwell's equations, AEFEM, residual type posteriori error estimator.

1 Introduction

Assuming a bounded, Lipschitz polygonal domain denoted as $\Omega \subset \mathbb{R}^2$ with a boundary $\partial\Omega$ and an inner interface denoted as Σ, where $\boldsymbol{n}$ represents the unit outward normal vector of $\partial\Omega$, and ν represents the normal vector of Σ. In this study, we investigate the

*Corresponding author.
Email: yangweixtu@126.com (W. Yang)

variable coefficient time-harmonic Maxwell's equations given by:

$$\begin{cases} \nabla\times\left(\mu_r^{-1}\nabla\times\boldsymbol{E}\right)-k^2\varepsilon_r\boldsymbol{E}=\boldsymbol{f} & \text{in } \Omega, \\ \boldsymbol{n}\times\boldsymbol{E}=0 & \text{on } \partial\Omega, \\ \left[\left[\nu\times\left(\mu_r^{-1}\nabla\times\boldsymbol{E}\right)\right]\right]_\Sigma=i\sigma_r^\Sigma\boldsymbol{E}_t & \text{on } \Sigma. \end{cases} \tag{1.1}$$

Here, $\boldsymbol{E}$ represents the electric field, $k>0$ is the wave number of the electromagnetic wave. The subscript t denotes the tangential part of the given vector, and $[[\cdot]]_\Sigma$ represents the jump over Σ, defined as:

$$\boldsymbol{f}_t=(\nu\times\boldsymbol{f})\times\nu \quad \text{and} \quad [[\boldsymbol{f}]]_\Sigma(\mathbf{x})=\lim_{s\to0^+}(\boldsymbol{f}(\mathbf{x}+s\nu)-\boldsymbol{f}(\mathbf{x}-s\nu)).$$

In the above equations, $\boldsymbol{f}\in[L^2(\Omega)]^2$ represents a given known function, $i=\sqrt{-1}$, μ_r represents the permeability, which is a positive bounded function with values bounded between M_1 and M_2. That is, $0<M_1\le\mu_r(x)\le M_2$ for all $x\in\Omega$. ε_r is a 2×2 symmetric positive definite (SPD) matrix. For any given $x\in\Omega$ and $\xi\in\mathbb{R}^2$, the following inequalities hold:

$$0<\lambda_1(x)|\xi|^2\le\xi\varepsilon_r(x)\xi^{\mathrm{T}}\le\lambda_2(x)|\xi|^2<\infty,$$

where λ_1 and λ_2 are the two eigenvalues of ε_r, satisfying $0<\lambda_1\le\lambda_2<\infty$. Additionally, σ_r^Σ represents an appropriately chosen surface conductivity, specifically used to represent graphene's surface conductivity. It is a matrix-valued and symmetric function denoted as $\sigma_r^\Sigma\in L^\infty(\Sigma)^{2\times2}$, possessing semidefinite real and complex parts and $\sigma_r^\Sigma=0$ on $\partial\Sigma$. Similar to ε_r, σ_r^Σ satisfies the bounded property: for any given $x\in\Omega$ and $\xi\in\mathbb{R}^2$, hold that:

$$0<M_3(x)|\xi|^2\le\xi\sigma_r^\Sigma(x)\xi^{\mathrm{T}}\le M_4(x)|\xi|^2<\infty.$$

Numerical solutions to Maxwell's equations play a crucial role in various applications. When it comes to solving Maxwell's equations numerically, there are several methods available, such as the finite difference time domain method [12, 27, 28] and the finite element method [1, 6, 13]. This paper primarily focuses on discussing the finite element method for solving Maxwell's equations, along with its adaptive mesh refinement technique [8, 14].

In the traditional finite element method, nodal basis functions are commonly used as a basis set for the finite element space. However, when dealing with electromagnetic field problems, the use of nodal basis functions can lead to incorrect solutions. One particular issue is the failure to satisfy the divergence condition. This discrepancy arises because we assume that $\boldsymbol{E}$ and $\boldsymbol{H}$ are quadratically differentiable during the integration by parts, while our nodal basis functions only fulfill the continuity condition. To overcome this challenge, Nédélec edge finite elements can be introduced, as discussed in [4, 5, 15]. These elements address the problem by incorporating edge-based basis functions that ensure the satisfaction of the divergence condition and provide accurate solutions for electromagnetic field problems.

In practical engineering and scientific computing applications, the propagation of electromagnetic fields can exhibit strong singularities [18]. One such phenomenon is the surface plasmon-polariton (SPP) [3, 16], which refers to a confined electromagnetic wave that decays slowly near a metal-air interface. SPP structures on "2D" materials like graphene [17], consisting of a monoatomic layer of carbon atoms in a hexagonal lattice, often have much shorter wavelengths compared to free-space radiation. The surface plasmon phenomenon finds applications in sensor technology, optical technology, photocatalysis, photoelectrochemistry, and nanophotonics [19–21].

However, the reduction in wavelength at the interface can introduce larger calculation errors. Employing a global refinement method to mitigate this issue would require significant computational resources. Therefore, we utilize a local refinement method known as the Adaptive Edge Finite Element Method (AEFEM) [2, 22]. While there have been numerous studies on the convergence of adaptive methods for the H^1 elliptic equation in recent years [7,23,24], research on the convergence of adaptive methods for Maxwell's equations is limited.

In [25] and [26], the convergence analysis of adaptive first-class Nédélec linear finite element methods for solving two-dimensional and three-dimensional $\mathbf{H}(\mathbf{curl};\Omega)$ elliptic equations is presented respectively, providing insights into the convergence properties of adaptive methods for Maxwell's equations.

In this process we use edge elements. The specific adaptation process is as follows:

$$\textbf{Solve} \rightarrow \textbf{Estimate} \rightarrow \textbf{Mark} \rightarrow \textbf{Refine}.$$

The paper is organized as follows: Section 2 introduces the construction of the posteriori error estimator. Section 3 establishes the lower bound of the posteriori error estimator. Section 4 proves the convergence of the Adaptive Edge Finite Element Method (AEFEM). Section 5 presents numerical experiments to validate the theory presented in the paper. Finally, Section 6 provides a summary of the paper.

2 Construction of posteriori error estimator

We introduce some notations and Sobolev spaces used in this paper.

$$\begin{aligned}
&\mathbf{H}(\mathbf{curl};\Omega) := \left\{\mathbf{v}\in[L^2(\Omega)]^2 : \nabla\times\mathbf{v}\in L^2(\Omega)\right\},\\
&\mathbf{H}_0(\mathbf{curl};\Omega) := \left\{\mathbf{v}\in\mathbf{H}(\mathbf{curl};\Omega) : \mathbf{v}\times\boldsymbol{n}=0 \text{ on } \partial\Omega\right\},\\
&\mathbf{X}(\Omega) := \left\{\mathbf{v}\in\mathbf{H}_0(\mathbf{curl};\Omega) : \mathbf{v}_t|_\Sigma\in[L^2(\Sigma)]^2\right\},\\
&\mathbf{H}_0^1(\Omega) := \left\{\mathbf{v} : \mathbf{v}\in[H_0^1(\Omega)]^2\right\}.
\end{aligned}$$

And the norm of space $\mathbf{X}(\Omega)$ is defined as following:

$$\begin{aligned}
\|\varphi\|_{\mathbf{X}_1(\Omega)} &= (\nabla\times\varphi,\nabla\times\varphi)_{0;\Omega}+(\varphi,\varphi)_{0;\Omega}+(\varphi_t,\varphi_t)_{0;\Sigma},\\
\|\varphi\|_{\mathbf{X}_2(\Omega)} &= \left(\mu_r^{-1}\nabla\times\varphi,\nabla\times\varphi\right)_{0;\Omega}+(\varepsilon_r\varphi,\varphi)_{0;\Omega}+\left(\sigma_r^{\Sigma}\varphi_t,\varphi_t\right)_{0;\Sigma}.
\end{aligned}$$

Here, we have $(v,w)_{0;\Omega}=\int_\Omega v\cdot\overline{w}dx$. Based on the properties of μ_r^{-1}, ε_r, and σ_r^Σ, we can observe the following property:

$$C_1\|p\|^2_{\mathbf{X}_1(\Omega)}\leq\|p\|^2_{\mathbf{X}_2(\Omega)}\leq C_2\|p\|^2_{\mathbf{X}_1(\Omega)},$$

where $C_1=\min\{\frac{1}{M_2},\lambda_1,M_3\}$ and $C_2=\max\{\frac{1}{M_1},\lambda_2,M_4\}$. Therefore, we can conclude that these two norms are equivalent. Consequently, we will use $\|\varphi\|_{\mathbf{X}(\Omega)}$ to represent this norm without distinction.

In general, when dealing with two mesh-dependent quantities M and N, we express the relationship as $M\lesssim N$, which means that there exists a constant $L>0$ independent of the mesh size h such that $M\leq LN$.

Now let's consider the variational and discrete variational forms of the original problem (1.1). First, the variational form of (1.1) is finding $\boldsymbol{E}\in\mathbf{X}(\Omega)$ such that the following equation holds:

$$\bar{a}(\boldsymbol{E},\psi)=(\boldsymbol{f},\psi)_{0;\Omega},\quad\forall\psi\in\mathbf{X}(\Omega).\tag{2.1}$$

Where the bilinear form $\bar{a}(\boldsymbol{E},\psi)$ is defined as following:

$$\bar{a}(\boldsymbol{E},\psi)=\left(\mu_r^{-1}\nabla\times\boldsymbol{E},\nabla\times\psi\right)_{0;\Omega}-(k^2\varepsilon_r\boldsymbol{E},\psi)_{0;\Omega}+i\left(\sigma_r^\Sigma\boldsymbol{E}_t,\psi_t\right)_{0;\Sigma}.$$

The existence and uniqueness of the solution to problem (2.1) have been studied in [10] under various conditions on the domain Ω and the coefficients ε_r and μ_r. For simplicity, let's assume that a unique solution exists for this variational problem. We can consider that these coefficients satisfy certain conditions, ensuring that the Babuška–Brezzi condition holds:

$$\sup_{0\neq\mathbf{v}\in\mathbf{X}(\Omega)}\frac{|\bar{a}(\boldsymbol{E},\mathbf{v})|}{\|\mathbf{v}\|_{\mathbf{X}(\Omega)}}\geq\beta\|\boldsymbol{E}\|_{\mathbf{X}(\Omega).}\tag{2.2}$$

Let $\mathcal{T}_k$ be a sequence of tetrahedral triangulations of the domain Ω. The finite element space $\mathcal{S}(\mathcal{T}_k)$ over $\mathcal{T}_k$ is defined as following:

$$\begin{aligned}\mathcal{S}(\mathcal{T}_k):=\{&\mathbf{u}\in\mathbf{H}(\mathbf{curl};\Omega):\mathbf{u}\times\nu|_{\partial\Omega}=\mathbf{0}\ \text{ and}\\&\mathbf{u}|_T=\mathbf{a}_T+\mathbf{b}_T\times\mathbf{x}\ \text{ with }\ \mathbf{a}_T\in\mathbb{R}^2,\ \mathbf{b}_T\in\mathbb{R},\ \forall T\in\mathcal{T}_k\}.\end{aligned}$$

Therefore, the discrete variational form of the original problem (1.1) is to find $\boldsymbol{E}_{\mathcal{T}_k}\in\mathcal{S}(\mathcal{T}_k)$ such that the following equation holds:

$$\bar{a}(\boldsymbol{E}_{\mathcal{T}_k},\psi)=(\boldsymbol{f},\psi)_{0;\Omega},\quad\forall\psi\in\mathcal{S}(\mathcal{T}_k).\tag{2.3}$$

In this paper, we utilize a posteriori error estimator of the residual type, which is derived from the coefficient functions and the numerical solution. We now define the

following element-wise residuals and edge-wise jump residuals associated with interior edges:

$$\begin{aligned}
&\eta_1(\boldsymbol{E}_{\mathcal{T}_k})|_\tau := \operatorname{div}\left(k^2\varepsilon_r\boldsymbol{E}_{\mathcal{T}_k}+\boldsymbol{f}\right)\big|_\tau,\\
&\eta_2(\boldsymbol{E}_{\mathcal{T}_k})|_e := \left[\left[\left(k^2\varepsilon_r\boldsymbol{E}_{\mathcal{T}_k}+\boldsymbol{f}\right)\cdot\nu\right]\right]_e,\\
&\eta_3(\boldsymbol{E}_{\mathcal{T}_k})|_{e_0} := \begin{cases} \operatorname{div}_\Sigma\left(i\sigma_r^\Sigma\boldsymbol{E}_{\mathcal{T}_k,t}\right)\big|_{e_0}, & e_0\subseteq\Sigma,\\ 0, & e_0\nsubseteq\Sigma, \end{cases}\\
&\eta_4(\boldsymbol{E}_{\mathcal{T}_k})|_\tau := \left(\boldsymbol{f}+k^2\varepsilon_r\boldsymbol{E}_{\mathcal{T}_k}-\nabla\times\mu_r^{-1}\nabla\times\boldsymbol{E}_{\mathcal{T}_k}\right)\Big|_\tau,\\
&\eta_5(\boldsymbol{E}_{\mathcal{T}_k})|_e := \left[\left[\mu_r^{-1}\nabla\times\boldsymbol{E}_{\mathcal{T}_k}\times\nu\right]\right]_e,\\
&\eta_6(\boldsymbol{E}_{\mathcal{T}_k})|_{e_0} := \begin{cases} \sigma_r^\Sigma\boldsymbol{E}_{\mathcal{T}_k,t}\big|_{e_0}, & e_0\subseteq\Sigma,\\ 0, & e_0\nsubseteq\Sigma. \end{cases}
\end{aligned}$$

It is important to note that $\eta_1(\boldsymbol{E}_{\mathcal{T}_k})$, $\eta_2(\boldsymbol{E}_{\mathcal{T}_k})$, $\eta_4(\boldsymbol{E}_{\mathcal{T}_k})$, and $\eta_5(\boldsymbol{E}_{\mathcal{T}_k})$ will be calculated once for each small cell τ. However, $\eta_3(\boldsymbol{E}_{\mathcal{T}_k})$ and $\eta_6(\boldsymbol{E}_{\mathcal{T}_k})$ will only be evaluated when $\partial\tau\cap\Sigma\neq\emptyset$. Here, we use $\mathcal{B}(\mathcal{T}_k)$ to represent the set of all inner edges in the triangulation $\mathcal{T}_k$.

We define the error indicator on element $\tau\in\mathcal{T}_k$ with respect to the finite element function $\boldsymbol{E}_{\mathcal{T}_k}\in\mathcal{S}(\mathcal{T}_k)$ as following:

$$\begin{aligned}
\eta_{\mathcal{T}_k}^2(\boldsymbol{E}_{\mathcal{T}_k},\tau) := &\sum_{e\in\tau\cap\mathcal{B}(\mathcal{T}_k)} h_\tau\left(\left\|\eta_2(\boldsymbol{E}_{\mathcal{T}_k})\right\|_{0;e}^2+\left\|\eta_5(\boldsymbol{E}_{\mathcal{T}_k})\right\|_{0;e}^2\right)\\
&+\sum_{e\in\tau\cap\mathcal{B}(\mathcal{T}_k)} h_\tau\left(\left\|\eta_3(\boldsymbol{E}_{\mathcal{T}_k})\right\|_{0;e}^2+\left\|\eta_6(\boldsymbol{E}_{\mathcal{T}_k})\right\|_{0;e}^2\right)\\
&+h_\tau^2\left(\left\|\eta_1(\boldsymbol{E}_{\mathcal{T}_k})\right\|_{0;\tau}^2+\left\|\eta_4(\boldsymbol{E}_{\mathcal{T}_k})\right\|_{0;\tau}^2\right),
\end{aligned}$$

where $|\tau|$ denotes the area of τ and $h_\tau=|\tau|^{\frac{1}{2}}$ denotes the size of the element τ. For a given subset $\mathcal{K}$ of $\mathcal{T}$, we can define the following equation:

$$\eta_{\mathcal{T}_k}^2(\boldsymbol{E}_{\mathcal{T}_k},\mathcal{K})=\sum_{\tau\in\mathcal{K}}\eta_{\mathcal{T}_k}^2(\boldsymbol{E}_{\mathcal{T}_k},\tau).$$

When $\mathcal{K}=\mathcal{T}_k$, the corresponding symbol can be simplified to $\eta(\boldsymbol{E}_{\mathcal{T}_k},\mathcal{T}_k)$. Let's assume that the k-th triangulation $\mathcal{T}_k$ and the corresponding finite element solution function $\boldsymbol{E}_{\mathcal{T}_k}\in\mathcal{S}(\mathcal{T}_k)$ of (2.3) are given. Then, for any element $\tau\in\mathcal{T}_k$, the error estimator $\eta_{\mathcal{T}_k}(\boldsymbol{E}_{\mathcal{T}_k},\tau)$ can be calculated. This is the estimation process in the standard adaptive process.

3 Lower bound estimate of posteriori error estimator

Now, one of our main objectives is to prove an lower bound estimate of the posteriori error estimator. To accomplish this, we need to introduce a decomposition lemma and a

corresponding approximation error estimate from [7], as well as another decomposition lemma from [8]. Additionally, we define the enlarged element patch as follows:

$$\tau^*:=\cup_{\tau'}\left\{\tau'\in\mathcal{T}_k:\tau'\cap\tau\neq\emptyset\right\},\quad e^*:=\cup_{e'}\left\{e'\in\mathcal{T}_k:e'\cap e\neq\emptyset\right\}.$$

Lemma 3.1 ([7, Theorem 2.3]). *For any $\mathbf{v}\in\mathbf{X}(\Omega)$, there exist $\varphi\in H_0^1(\Omega)$ and $\mathbf{v}_s\in\mathbf{H}_0^1(\Omega)$ such that*

$$\mathbf{v}=\nabla\varphi+\mathbf{v}_s\quad in\ \ \Omega, \tag{3.1a}$$

$$\|\varphi\|_{1;\Omega}+\|\mathbf{v}_s\|_{1;\Omega}\leq C\|\mathbf{v}\|_{\mathbf{X}(\Omega)}, \tag{3.1b}$$

where the constant C depends only on $\mathbf{X}(\Omega)$.

Lemma 3.2 ([7, Interpolation theorem]). *There exists a interpolation operator $\mathcal{I}_k: H_0^1(\Omega)\to V_k$, where V_k is the piecewise linear H_0^1-conforming finite element space over $\mathcal{T}_k$ defined by*

$$V_k:=\left\{v\in H_0^1(\Omega):v|_\tau=a_\tau+\mathbf{b}_\tau\cdot\mathbf{x}\ \text{with}\ a_\tau\in\mathbb{R}\ \text{and}\ \mathbf{b}_\tau\in\mathbb{R}^2,\ \forall\tau\in\mathcal{T}_k\right\}.$$

The interpolation operator satisfies the following properties:

$$\begin{cases}\mathcal{I}_k\phi_h=\phi_h, & \forall\phi_h\in V_k,\\ \|\nabla\mathcal{I}_k\phi\|_{0;\tau}\leq C|\phi|_{1;\tau^*},\\ \|\phi-\mathcal{I}_k\phi\|_{0;\tau}\leq Ch_\tau|\phi|_{1;\tau^*},\\ \|\phi-\mathcal{I}_k\phi\|_{0;e}\leq Ch_e^{\frac{1}{2}}|\phi|_{1;e^*}.\end{cases} \tag{3.2}$$

Lemma 3.3 ([9, Theorem 1]). *There exists an operator $\Pi_k:\mathbf{H}_0^1(\Omega)\to\mathcal{S}(\mathcal{T}_k)$ with the following properties: For every $\mathbf{u}\in\mathbf{H}_0^1(\Omega)$ there exists $\phi\in H_0^1(\Omega)$ and $\boldsymbol{w}\in\mathbf{H}_0^1(\Omega)$ such that*

$$\mathbf{u}-\Pi_k\mathbf{u}=\nabla\phi+\boldsymbol{w}. \tag{3.3}$$

The decomposition satisfies

$$h_\tau^{-1}\|\phi\|_{0;\tau}+\|\nabla\phi\|_{0;\tau}\leq C\|\mathbf{u}\|_{0;\tau^*}, \tag{3.4a}$$

$$h_\tau^{-1}\|\boldsymbol{w}\|_{0;\tau}+\|\nabla\boldsymbol{w}\|_{0;\tau}\leq C\|\nabla\times\mathbf{u}\|_{0;\tau^*}. \tag{3.4b}$$

The constant C depends only on the shape of the elements in the enlarged element patch τ^*.

Now, we can present a theorem providing a lower bound estimate for the error estimator.

Theorem 3.1. *Assume $\boldsymbol{E}\in\mathbf{X}(\Omega)$ be the solution of* (2.1)*, $\mathcal{T}_k$ denotes the k-th mesh, and $\boldsymbol{E}_{\mathcal{T}_k}\in S(\mathcal{T}_k)$ be the discrete solution of* (2.3)*. Then have a constant $C>0$ relying only on wave number k and the bounded properties of μ_r^{-1}, ε_r and σ_r^{Σ}, such that*

$$\left\|\boldsymbol{E}-\boldsymbol{E}_{\mathcal{T}_k}\right\|_{\mathbf{X}(\Omega)}^2\leq C\eta^2(\boldsymbol{E}_{\mathcal{T}_k},\mathcal{T}_k).$$

Proof. By utilizing the Babuška–Brezzi condition (2.2) and Lemma 3.1, we obtain:

$$\begin{aligned}\|\boldsymbol{E}-\boldsymbol{E}_{\mathcal{T}_k}\|_{\mathbf{X}(\Omega)} \leq & \beta^{-1} \sup_{0\neq \mathbf{v}\in \mathbf{X}(\Omega)} \frac{|\bar{a}(\boldsymbol{E}-\boldsymbol{E}_{\mathcal{T}_k},\mathbf{v})|}{\|\mathbf{v}\|_{\mathbf{X}(\Omega)}} \\ = & \beta^{-1} \sup_{0\neq \mathbf{v}\in \mathbf{X}(\Omega)} \frac{|\bar{a}(\boldsymbol{E}-\boldsymbol{E}_{\mathcal{T}_k},\nabla\varphi+\mathbf{v}_{\boldsymbol{s}})|}{\|\mathbf{v}\|_{\mathbf{X}(\Omega)}}.\end{aligned}$$

By applying the bilinearity of $\bar{a}(\cdot,\cdot)$, we can divide the above estimate into two parts for further analysis. Let's first consider the first part. Because of $\sigma_r^{\Sigma}=0$ on $\partial\Sigma$ we have

$$\int_{\partial\Sigma}\left(i\sigma_r^{\Sigma}\boldsymbol{E}_{\mathcal{T}_{k,t}}\right)\overline{(\varphi-\mathcal{I}_k\varphi)_t}=0.$$

Using techniques such as integral by parts, Galerkin orthogonality, and the Cauchy-Schwarz inequality, we obtain:

$$\begin{aligned}&\left|\bar{a}(\boldsymbol{E}-\boldsymbol{E}_{\mathcal{T}_k},\nabla\varphi)\right|=\left|\bar{a}(\boldsymbol{E}-\boldsymbol{E}_{\mathcal{T}_k},\nabla\varphi-\nabla\mathcal{I}_k\varphi)\right| \\ =&\left|\sum_{\tau\in\mathcal{T}_k}\int_{\tau}\left(k^2\varepsilon_r\boldsymbol{E}_{\mathcal{T}_k}+\boldsymbol{f}\right)\overline{(\nabla\varphi-\nabla\mathcal{I}_k\varphi)}-\sum_{e_0\subset\Sigma}\int_{e_0}\left(i\sigma_r^{\Sigma}\boldsymbol{E}_{\mathcal{T}_k,t}\right)\overline{(\nabla\varphi-\nabla\mathcal{I}_k\varphi)_t}\right| \\ =&\left|-\sum_{\tau\in\mathcal{T}_k}\int_{\tau}\operatorname{div}\left(k^2\varepsilon_r\boldsymbol{E}_{\mathcal{T}_k}+\boldsymbol{f}\right)\overline{(\varphi-\mathcal{I}_k\varphi)}+\sum_{e\in\mathcal{B}(\mathcal{T}_k)}\int_e\left[\left[\left(k^2\varepsilon_r\boldsymbol{E}_{\mathcal{T}_k}+\boldsymbol{f}\right)\cdot\nu\right]\right]_e\overline{(\varphi-\mathcal{I}_k\varphi)}\right. \\ &\left.+\sum_{e_0\subset\Sigma}\int_{e_0}\operatorname{div}_{\Sigma}\left(i\sigma_r^{\Sigma}\boldsymbol{E}_{\mathcal{T}_k,t}\right)\overline{(\varphi-\mathcal{I}_k\varphi)}-\int_{\partial\Sigma}\nu_{\Sigma}\cdot\left(i\sigma_r^{\Sigma}\boldsymbol{E}_{\mathcal{T}_k,t}\right)\overline{(\varphi-\mathcal{I}_k\varphi)}\right| \\ =&\left|-\sum_{\tau\in\mathcal{T}_k}\int_{\tau}\operatorname{div}\left(k^2\varepsilon_r\boldsymbol{E}_{\mathcal{T}_k}+\boldsymbol{f}\right)\overline{(\varphi-\mathcal{I}_k\varphi)}+\sum_{e\in\mathcal{B}(\mathcal{T}_k)}\int_e\left[\left[\left(k^2\varepsilon_r\boldsymbol{E}_{\mathcal{T}_k}+\boldsymbol{f}\right)\cdot\nu\right]\right]_e\overline{(\varphi-\mathcal{I}_k\varphi)}\right. \\ &\left.+\sum_{e_0\subset\Sigma}\int_{e_0}\operatorname{div}_{\Sigma}\left(i\sigma_r^{\Sigma}\boldsymbol{E}_{\mathcal{T}_k,t}\right)\overline{(\varphi-\mathcal{I}_k\varphi)}\right| \\ \leq&\sum_{\tau\in\mathcal{T}_k}\left\|\eta_1(\boldsymbol{E}_{\mathcal{T}_k})\right\|_{0;\tau}\|\varphi-\mathcal{I}_k\varphi\|_{0;\tau}+\sum_{e\in\mathcal{B}(\mathcal{T}_k)}\left\|\eta_2(\boldsymbol{E}_{\mathcal{T}_k})\right\|_{0;e}\|\varphi-\mathcal{I}_k\varphi\|_{0;e} \\ &+\sum_{e_0\subset\Sigma}\left\|\eta_3(\boldsymbol{E}_{\mathcal{T}_k})\right\|_{0;e_0}\|\varphi-\mathcal{I}_k\varphi\|_{0;e_0}.\end{aligned}$$

Using the estimate of (3.1), (3.2) and the regularity of mesh $\mathcal{T}_k$ we have:

$$\begin{aligned}\left|\bar{a}(\boldsymbol{E}-\boldsymbol{E}_{\mathcal{T}_k},\nabla\varphi)\right|\lesssim&\sum_{\tau\in\mathcal{T}_k}h_{\tau}\left\|\eta_1(\boldsymbol{E}_{\mathcal{T}_k})\right\|_{0;\tau}|\varphi|_{1;\tau^*}+\sum_{e\in\mathcal{B}(\mathcal{T}_k)}h_e^{\frac{1}{2}}\left\|\eta_2(\boldsymbol{E}_{\mathcal{T}_k})\right\|_{0;e}|\varphi|_{1;e} \\ &+\sum_{e_0\subset\Sigma}h_e^{\frac{1}{2}}\left\|\eta_3(\boldsymbol{E}_{\mathcal{T}_k})\right\|_{0;e_0}|\varphi|_{1;e_0} \\ \lesssim&\eta(\boldsymbol{E}_{\mathcal{T}_k},\mathcal{T}_k)\|\mathbf{v}\|_{\mathbf{X}(\Omega)}.\end{aligned}$$

Subsequently, we direct our attention to the second constituent. Initially, we invoke Lemma 3.3 to establish a decomposition of $\mathbf{v}_s=\nabla\phi+\boldsymbol{n}$. Concerning the component associated with $\nabla\phi$, we proceed by employing Cauchy's inequality and the trace inequality, leading to the following result:

$$\begin{aligned}
&\left|\overline{a}(\boldsymbol{E}-\boldsymbol{E}_{\mathcal{T}_k},\nabla\phi)\right|\\
=&\left|\sum_{\tau\in\mathcal{T}_k}\int_\tau\left(k^2\varepsilon_r\boldsymbol{E}_{\mathcal{T}_k}+\boldsymbol{f}\right)\overline{(\nabla\phi)}-\sum_{e_0\subset\Sigma}\int_{e_0}\left(i\sigma_r^\Sigma\boldsymbol{E}_{\mathcal{T}_k,t}\right)\overline{(\nabla\phi)_t}\right|\\
=&\left|-\sum_{\tau\in\mathcal{T}_k}\int_\tau\operatorname{div}\left(k^2\varepsilon_r\boldsymbol{E}_{\mathcal{T}_k}+\boldsymbol{f}\right)\cdot\overline{\phi}+\sum_{e\in\mathcal{B}(\mathcal{T}_k)}\int_e\left[\left[\left(k^2\varepsilon_r\boldsymbol{E}_{\mathcal{T}_k}+\boldsymbol{f}\right)\cdot\nu\right]\right]_e\cdot\overline{\phi}\right.\\
&\quad\left.+\sum_{e_0\subset\Sigma}\int_{e_0}\operatorname{div}_\Sigma\left(i\sigma_r^\Sigma\boldsymbol{E}_{\mathcal{T}_k,t}\right)\cdot\overline{\phi}-\int_{\partial\Sigma}\nu_\Sigma\cdot\left(i\sigma_r^\Sigma\boldsymbol{E}_{\mathcal{T}_k,t}\right)\overline{\phi}\right|\\
\le&\sum_{\tau\in\mathcal{T}_k}\left\|\eta_1(\boldsymbol{E}_{\mathcal{T}_k})\right\|_{0;\tau}\|\phi\|_{0;\tau}+\sum_{e\in\mathcal{B}(\mathcal{T}_k)}\left\|\eta_2(\boldsymbol{E}_{\mathcal{T}_k})\right\|_{0;e}\|\phi\|_{0;e}+\sum_{e_0\subset\Sigma}\left\|\eta_3(\boldsymbol{E}_{\mathcal{T}_k})\right\|_{0;e_0}\|\phi\|_{0;e_0}\\
\le&\sum_{\tau\in\mathcal{T}_k}h_\tau\left\|\eta_1(\boldsymbol{E}_{\mathcal{T}_k})\right\|_{0;\tau}h_\tau^{-1}\|\phi\|_{0;\tau}+\sum_{e\in\mathcal{B}(\mathcal{T}_k)}\left\|\eta_2(\boldsymbol{E}_{\mathcal{T}_k})\right\|_{0;e}\left(h_\tau^{-\frac{1}{2}}\|\phi\|_{0;\tau}+h_\tau^{\frac{1}{2}}\|\nabla\phi\|_{0;\tau}\right)\\
&\quad+\sum_{e_0\subset\Sigma}\left\|\eta_3(\boldsymbol{E}_{\mathcal{T}_k})\right\|_{0;e_0}\left(h_\tau^{-\frac{1}{2}}\|\phi\|_{0;\tau}+h_\tau^{\frac{1}{2}}\|\nabla\phi\|_{0;\tau}\right).
\end{aligned}$$

Then use the estimate of (3.1), (3.4):

$$\begin{aligned}
&\left|\overline{a}(\boldsymbol{E}-\boldsymbol{E}_{\mathcal{T}_k},\nabla\phi)\right|\\
\le&\sum_{\tau\in\mathcal{T}_k}\eta_{\mathcal{T}_k}(\boldsymbol{E}_{\mathcal{T}_k},\tau)h_\tau^{-1}\|\phi\|_{0;\tau}+\sum_{\tau\in\mathcal{T}_k}\eta_{\mathcal{T}_k}(\boldsymbol{E}_{\mathcal{T}_k},\tau)\left(h_\tau^{-1}\|\phi\|_{0;\tau}+\|\nabla\phi\|_{0;\tau}\right)\\
&\quad+\sum_{\tau\in\mathcal{T}_k}\eta_{\mathcal{T}_k}(\boldsymbol{E}_{\mathcal{T}_k},\tau)\left(h_\tau^{-1}\|\phi\|_{0;\tau}+\|\nabla\phi\|_{0;\tau}\right)\\
\lesssim&\eta(\boldsymbol{E}_{\mathcal{T}_k},\mathcal{T}_k)\|\mathbf{v}_s\|_{0;\Omega}\lesssim\eta(\boldsymbol{E}_{\mathcal{T}_k},\mathcal{T}_k)\|\mathbf{v}_s\|_{1;\Omega}\lesssim\eta(\boldsymbol{E}_{\mathcal{T}_k},\mathcal{T}_k)\|\mathbf{v}\|_{\mathbf{X}(\Omega)}.
\end{aligned}$$

As for the part of $\boldsymbol{w}$, we use integral by parts, Galerkin orthogonality and Cauchy–Schwarz inequality we have:

$$\begin{aligned}
|\overline{a}(\boldsymbol{E}-\boldsymbol{E}_{\mathcal{T}_k},\boldsymbol{w})|=&\sum_{\tau\in\mathcal{T}_k}\int_\tau\left(\boldsymbol{f}+k^2\varepsilon_r\boldsymbol{E}_{\mathcal{T}_k}-\nabla\times\mu_r^{-1}\nabla\times\boldsymbol{E}_{\mathcal{T}_k}\right)\cdot\overline{\boldsymbol{w}}\\
&+\sum_{e\in\mathcal{B}(\mathcal{T}_k)}\int_e\left[\left[\nu\times\mu_r^{-1}\nabla\times\boldsymbol{E}_{\mathcal{T}_k}\right]\right]e\cdot\overline{\boldsymbol{w}}+\sum_{e_0\subset\Sigma}\int_{e_0}\left(i\sigma_r^\Sigma\boldsymbol{E}_{\mathcal{T}_k,t}\right)\cdot\overline{\boldsymbol{w}_t}\\
\le&\sum_{\tau\in\mathcal{T}_k}\left\|\boldsymbol{f}+k^2\varepsilon_r\boldsymbol{E}_{\mathcal{T}_k}-\nabla\times\mu_r^{-1}\nabla\times\boldsymbol{E}_{\mathcal{T}_k}\right\|_{0;\tau}\|\boldsymbol{w}\|_{0;\tau}\\
&+\sum_{e\in\mathcal{B}(\mathcal{T}_k)}\left\|\left[\left[\mu_r^{-1}\nabla\times\boldsymbol{E}_{\mathcal{T}_k}\times\nu\right]\right]e\right\|_{0;e}\|\boldsymbol{w}\|_{0;e}+\sum_{e_0\subset\Sigma}\int_{e_0}\left\|i\sigma_r^\Sigma\boldsymbol{E}_{\mathcal{T}_k,t}\right\|_{0;e_0}\|\boldsymbol{w}\|_{0;e_0}.
\end{aligned}$$

Subsequently, by utilizing the trace inequality and the estimate from (3.1) and (3.4), we can deduce the following inequality:

$$\begin{aligned}
|\bar{a}(\boldsymbol{E}-\boldsymbol{E}_{\mathcal{T}_k},\boldsymbol{w})| \leq & \sum_{\tau\in\mathcal{T}_k}\left\|\boldsymbol{f}+k^2\varepsilon_r\boldsymbol{E}_{\mathcal{T}_k}-\nabla\times\mu_r^{-1}\nabla\times\boldsymbol{E}_{\mathcal{T}_k}\right\|_{0;\tau}\|\boldsymbol{w}\|_{0;\tau} \\
& +\sum_{e\in\mathcal{B}(\mathcal{T}_k)}\left\|\left[\left[\mu_r^{-1}\nabla\times\boldsymbol{E}_{\mathcal{T}_k}\times\nu\right]\right]e\right\|_{0;e}\|\boldsymbol{w}\|_{0;e}+\sum_{e_0\subset\Sigma}\int_{e_0}\left\|i\sigma_r^{\Sigma}\boldsymbol{E}_{\mathcal{T}_k,t}\right\|_{0;e_0}\|\boldsymbol{w}\|_{0;e_0} \\
\leq & \sum_{\tau\in\mathcal{T}_k}\eta_{\mathcal{T}_k}(\boldsymbol{E}_{\mathcal{T}_k},\tau)h_\tau^{-1}\|\boldsymbol{w}\|_{0;\tau}+\sum_{\tau\in\mathcal{T}_k}\eta_{\mathcal{T}_k}(\boldsymbol{E}_{\mathcal{T}_k},\tau)\left(h_\tau^{-1}\|\boldsymbol{w}\|_{0;\tau}+\|\nabla\boldsymbol{w}\|_{0;\tau}\right) \\
& +\sum_{\tau\in\mathcal{T}_k}\eta_{\mathcal{T}_k}(\boldsymbol{E}_{\mathcal{T}_k},\tau)\left(h_\tau^{-1}\|\boldsymbol{w}\|_{0;\tau}+\|\nabla\boldsymbol{w}\|_{0;\tau}\right) \\
\lesssim & \eta(\boldsymbol{E}_{\mathcal{T}_k},\mathcal{T}_k)\|\mathbf{v}_{\boldsymbol{s}}\|_{0;\Omega}\lesssim\eta(\boldsymbol{E}_{\mathcal{T}_k},\mathcal{T}_k)\|\mathbf{v}_{\boldsymbol{s}}\|_{1;\Omega}\lesssim\eta(\boldsymbol{E}_{\mathcal{T}_k},\mathcal{T}_k)\|\mathbf{v}\|_{\mathbf{X}(\Omega)}.
\end{aligned}$$

Combine the above we have:

$$|\bar{a}(\boldsymbol{E}-\boldsymbol{E}_{\mathcal{T}_k},\boldsymbol{w})|\lesssim\eta(\boldsymbol{E}_{\mathcal{T}_k},\mathcal{T}_k)\|\mathbf{v}\|_{\mathbf{X}(\Omega)}, \tag{3.5a}$$

$$|\bar{a}(\boldsymbol{E}-\boldsymbol{E}_{\mathcal{T}_k},\nabla\phi)|\lesssim\eta(\boldsymbol{E}_{\mathcal{T}_k},\mathcal{T}_k)\|\mathbf{v}\|_{\mathbf{X}(\Omega)}, \tag{3.5b}$$

$$|\bar{a}(\boldsymbol{E}-\boldsymbol{E}_{\mathcal{T}_k},\nabla\varphi)|\lesssim\eta(\boldsymbol{E}_{\mathcal{T}_k},\mathcal{T}_k)\|\mathbf{v}\|_{\mathbf{X}(\Omega)}. \tag{3.5c}$$

Therefore we can get the following inequality:

$$|\bar{a}(\boldsymbol{E}-\boldsymbol{E}_{\mathcal{T}_k},\mathbf{v})|\lesssim\eta(\boldsymbol{E}_{\mathcal{T}_k},\mathcal{T}_k)\|\mathbf{v}\|_{\mathbf{X}(\Omega)}. \tag{3.6}$$

Now we have:

$$\begin{aligned}
\|\boldsymbol{E}-\boldsymbol{E}_{\mathcal{T}_k}\|_{\mathbf{X}(\Omega)} \leq & \beta^{-1}\sup_{0\neq\mathbf{v}\in\mathbf{X}(\Omega)}\frac{|\bar{a}(\boldsymbol{E}-\boldsymbol{E}_{\mathcal{T}_k},\mathbf{v})|}{\|\mathbf{v}\|_{\mathbf{X}(\Omega)}} \\
\lesssim & \eta(\boldsymbol{E}_{\mathcal{T}_k},\mathcal{T}_k)\leq C\eta(\boldsymbol{E}_{\mathcal{T}_k},\mathcal{T}_k).
\end{aligned}$$

Proof completed. □

4 Convergence of the AEFEM

In this section, our objective is to prove the convergence of the AEFEM (Adaptive Edge Finite Element Method). We will begin by constructing an auxiliary estimator, which will be used to quantify the error in the numerical approximation. Next, we will prove an auxiliary theorem that establishes a relationship between the auxiliary estimator and the error. Finally, by combining the auxiliary theorem with the estimator, we will provide a rigorous proof of the convergence of the AEFEM, demonstrating that the numerical solution converges to the exact solution as the mesh is refined.

4.1 Contraction of the error estimator

In this subsection, our first step is to construct an auxiliary estimator. We will then proceed to prove the convergence properties of this error estimator. To begin, we define the weighted maximum-norm of the coefficients μ_r^{-1} and ε_r on an element τ as follows:

$$\eta^2_{\mathcal{T}_k}(G,\tau):=h_\tau^2\left(\|m\|^2_{\infty;\tau}+h_\tau^{-2}\left\|\mu_r^{-1}\right\|^2_{\infty;\tau^*}+\|\mathrm{div}\varepsilon_r\|^2_{\infty;\tau}+h_\tau^{-2}\|\varepsilon_r\|^2_{\infty;\tau^*}+h_\tau^{-1}+h_\tau^{-2}\right).$$

Here, $m=(\frac{\partial\mu_r^{-1}}{\partial y},-\frac{\partial\mu_r^{-1}}{\partial x})^T$, $e_0\subset\Sigma$, and $\sigma_r^\Sigma\equiv 0$ outside e_0. For a given subset $\mathcal{K}\subseteq\mathcal{T}_k$, we can define the following equation:

$$\eta_{\mathcal{T}_k}(G,\mathcal{K}):=\max_{\tau\in\mathcal{K}}\eta_{\mathcal{T}_k}(G,\tau).$$

In particular, if $\mathcal{K}=\mathcal{T}_k$, we can simplify the previously defined symbols. We denote $\eta(G,\mathcal{T}_k)$ as $\eta_{\mathcal{T}_k}(G,\mathcal{T}_k)$. Based on the above definitions, it is evident that the monotonicity of the following inequalities is clearly established:

$$\eta(G,\mathcal{T}_{k+1})\leq\eta(G,\mathcal{T}_k)\leq\eta(G,\mathcal{T}_0),$$

where $\mathcal{T}_0$ represents the initial mesh. Now in this following lemma we consider the effect of the finite element solution on the error indicator when the finite element mesh is invariant. For the proof of the lemma, we mainly refer to the paper [8]. On this basis, we added the estimator on interface to the proof.

Lemma 4.1. *Let $\mathcal{T}_k$, $\mathcal{T}_{k+1}$ denote the k-th mesh and the $(k+1)$-th mesh, where $\mathcal{T}_{k+1}$ is obtained by refining $\mathcal{T}_k$ once. Assume $\boldsymbol{E}_{\mathcal{T}_k}\in\mathcal{S}(\mathcal{T}_k)$ and $\boldsymbol{E}_{\mathcal{T}_{k+1}}\in\mathcal{S}(\mathcal{T}_{k+1})$ are the discrete finite element solutions of the problem* (2.3)*. For any given $\alpha>0$, there exists a constant C_α that depends on the region Ω, the properties of ε_r, μ_r^{-1}, and α. This constant ensures the validity of the following inequality:*

$$\eta^2\left(\boldsymbol{E}_{\mathcal{T}_{k+1}},\mathcal{T}_{k+1}\right)\leq(1+\alpha)\eta^2\left(\boldsymbol{E}_{\mathcal{T}_k},\mathcal{T}_{k+1}\right)+C_\alpha\left\|\boldsymbol{E}_{\mathcal{T}_{k+1}}-\boldsymbol{E}_{\mathcal{T}_k}\right\|^2_{\mathbf{X}(\Omega)}.$$

Proof. Following the proof method of [8, Lemma 6], we can similarly obtain the following results: for any element $\tau_*\in\mathcal{T}_{k+1}$ and $e_*=\tau_*^1\cap\tau_*^2$ with $\tau_*^1,\tau_*^2\in\mathcal{T}_{k+1}$, hold that

$$\begin{aligned}
&h_{\tau_*}\left\|\eta_1\left(\boldsymbol{E}_{\mathcal{T}_{k+1}}\right)\right\|_{0;\tau_*}\lesssim h_{\tau_*}\left\|\eta_1\left(\boldsymbol{E}_{\mathcal{T}_k}\right)\right\|_{0;\tau_*}+\eta_{\mathcal{T}_{k+1}}(G,\tau_*)\left\|\boldsymbol{E}_{\mathcal{T}_k}-\boldsymbol{E}_{\mathcal{T}_{k+1}}\right\|_{\mathrm{curl};\tau_*},\\
&h_{\tau_*}\left\|\eta_4\left(\boldsymbol{E}_{\mathcal{T}_{k+1}}\right)\right\|_{0;\tau_*}\lesssim h_{\tau_*}\left\|\eta_4\left(\boldsymbol{E}_{\mathcal{T}_k}\right)\right\|_{0;\tau_*}+\eta_{\mathcal{T}_{k+1}}(G,\tau_*)\left\|\boldsymbol{E}_{\mathcal{T}_k}-\boldsymbol{E}_{\mathcal{T}_{k+1}}\right\|_{\mathrm{curl};\tau_*},\\
&h^{\frac{1}{2}}_{\tau_*}\left\|\eta_2\left(\boldsymbol{E}_{\mathcal{T}_{k+1}}\right)\right\|_{0;e_*}\lesssim h^{\frac{1}{2}}_{\tau_*}\left\|\eta_2\left(\boldsymbol{E}_{\mathcal{T}_k}\right)\right\|_{0;e_*}+\eta_{\mathcal{T}_{k+1}}(G,\tau_*)\left\|\left(\boldsymbol{E}_{\mathcal{T}_k}-\boldsymbol{E}_{\mathcal{T}_{k+1}}\right)\right\|_{0;\tau_*^1\cup\tau_*^2},\\
&h^{\frac{1}{2}}_{\tau_*}\left\|\eta_5\left(\boldsymbol{E}_{\mathcal{T}_{k+1}}\right)\right\|_{0;e_*}\lesssim h^{\frac{1}{2}}_{\tau_*}\left\|\eta_5\left(\boldsymbol{E}_{\mathcal{T}_k}\right)\right\|_{0;e_*}+\eta_{\mathcal{T}_{k+1}}(G,\tau_*)\left\|\nabla\times\left(\boldsymbol{E}_{\mathcal{T}_k}-\boldsymbol{E}_{\mathcal{T}_{k+1}}\right)\right\|_{0;\tau_*^1\cup\tau_*^2}.
\end{aligned}$$

where $\|\cdot\|_{curl}:=\left(\|\cdot\|_0^2+\|\nabla\times\cdot\|_0^2\right)^{\frac{1}{2}}$.

Consider the error estimator $\eta_3(\boldsymbol{E}_{\mathcal{T}_{k+1}})$ and $\eta_6(\boldsymbol{E}_{\mathcal{T}_{k+1}})$ on the interface. Applying the definition of $\eta_3(\boldsymbol{E}_{\mathcal{T}_{k+1}})$, $\eta_3(\boldsymbol{E}_{\mathcal{T}_{k+1}})$, the triangle inequality and the inverse inequality we obtain:

$$\begin{aligned}
h_{\tau_*}^{\frac{1}{2}}\left\|\eta_3(\boldsymbol{E}_{\mathcal{T}_{k+1}})\right\|_{0;e_*} &\leq h_{\tau_*}^{\frac{1}{2}}\left\|\eta_3(\boldsymbol{E}_{\mathcal{T}_k})\right\|_{0;e_*}+h_{\tau_*}^{\frac{1}{2}}\left\|\mathrm{div}_\Sigma\left(i\sigma_r^\Sigma\left(\boldsymbol{E}_{\mathcal{T}_k,t}-\boldsymbol{E}_{\mathcal{T}_{k+1},t}\right)\right)\right\|_{0;e_*}\\
&\leq h_{\tau_*}^{\frac{1}{2}}\left\|\eta_3(\boldsymbol{E}_{\mathcal{T}_k})\right\|_{0;e_*}+\left\|i\sigma_r^\Sigma\left(\boldsymbol{E}_{\mathcal{T}_k,t}-\boldsymbol{E}_{\mathcal{T}_{k+1},t}\right)\right\|_{0;e_*}\\
&\leq h_{\tau_*}^{\frac{1}{2}}\left\|\eta_3(\boldsymbol{E}_{\mathcal{T}_k})\right\|_{0;e_*}+\eta_{\mathcal{T}_{k+1}}(G,\tau_*)\left\|i\sigma_r^\Sigma\left(\boldsymbol{E}_{\mathcal{T}_k,t}-\boldsymbol{E}_{\mathcal{T}_{k+1},t}\right)\right\|_{0;e_*},\\
h_{\tau_*}^{\frac{1}{2}}\left\|\eta_6(\boldsymbol{E}_{\mathcal{T}_{k+1}})\right\|_{0;e_*} &\leq h_{\tau_*}^{\frac{1}{2}}\left\|\eta_6(\boldsymbol{E}_{\mathcal{T}_k})\right\|_{0;e_*}+h_{\tau_*}^{\frac{1}{2}}\left\|i\sigma_r^\Sigma\left(\boldsymbol{E}_{\mathcal{T}_k,t}-\boldsymbol{E}_{\mathcal{T}_{k+1},t}\right)\right\|_{0;e_*}\\
&\leq h_{\tau_*}^{\frac{1}{2}}\left\|\eta_6(\boldsymbol{E}_{\mathcal{T}_k})\right\|_{0;e_*}+\eta_{\mathcal{T}_{k+1}}(G,\tau_*)\left\|i\sigma_r^\Sigma\left(\boldsymbol{E}_{\mathcal{T}_k,t}-\boldsymbol{E}_{\mathcal{T}_{k+1},t}\right)\right\|_{0;e_*}.
\end{aligned}$$

By summarizing all the above results, we obtain:

$$\begin{aligned}
&h_{\tau_*}\left\|\eta_1\left(\boldsymbol{E}_{\mathcal{T}_{k+1}}\right)\right\|_{0;\tau_*}\lesssim h_{\tau_*}\left\|\eta_1\left(\boldsymbol{E}_{\mathcal{T}_k}\right)\right\|_{0;\tau_*}+\eta_{\mathcal{T}_{k+1}}(G,\tau_*)\left\|\boldsymbol{E}_{\mathcal{T}_k}-\boldsymbol{E}_{\mathcal{T}_{k+1}}\right\|_{0;\tau_*},\\
&h_{\tau_*}^{\frac{1}{2}}\left\|\eta_2\left(\boldsymbol{E}_{\mathcal{T}_{k+1}}\right)\right\|_{0;e_*}\lesssim h_{\tau_*}^{\frac{1}{2}}\left\|\eta_2\left(\boldsymbol{E}_{\mathcal{T}_k}\right)\right\|_{0;e_*}+\eta_{\mathcal{T}_{k+1}}(G,\tau_*)\left\|\left(\boldsymbol{E}_{\mathcal{T}_k}-\boldsymbol{E}_{\mathcal{T}_{k+1}}\right)\right\|_{0;\tau_*^1\cup\tau_*^2},\\
&h_{\tau_*}^{\frac{1}{2}}\left\|\eta_3(\boldsymbol{E}_{\mathcal{T}_{k+1}})\right\|_{0;e_*}\lesssim h_{\tau_*}^{\frac{1}{2}}\left\|\eta_3(\boldsymbol{E}_{\mathcal{T}_k})\right\|_{0;e_*}+\eta_{\mathcal{T}_{k+1}}(G,\tau_*)\left\|i\sigma_r^\Sigma\left(\boldsymbol{E}_{\mathcal{T}_k,t}-\boldsymbol{E}_{\mathcal{T}_{k+1},t}\right)\right\|_{0;e_*},\\
&h_{\tau_*}\left\|\eta_4\left(\boldsymbol{E}_{\mathcal{T}_{k+1}}\right)\right\|_{0;\tau_*}\lesssim h_{\tau_*}\left\|\eta_4\left(\boldsymbol{E}_{\mathcal{T}_k}\right)\right\|_{0;\tau_*}+\eta_{\mathcal{T}_{k+1}}(G,\tau_*)\left\|\boldsymbol{E}_{\mathcal{T}_k}-\boldsymbol{E}_{\mathcal{T}_{k+1}}\right\|_{\mathrm{curl};\tau_*},\\
&h_{\tau_*}^{\frac{1}{2}}\left\|\eta_5\left(\boldsymbol{E}_{\mathcal{T}_{k+1}}\right)\right\|_{0;e_*}\lesssim h_{\tau_*}^{\frac{1}{2}}\left\|\eta_5\left(\boldsymbol{E}_{\mathcal{T}_k}\right)\right\|_{0;e_*}+\eta_{\mathcal{T}_{k+1}}(G,\tau_*)\left\|\nabla\times\left(\boldsymbol{E}_{\mathcal{T}_k}-\boldsymbol{E}_{\mathcal{T}_{k+1}}\right)\right\|_{0;\tau_*^1\cup\tau_*^2},\\
&h_{\tau_*}^{\frac{1}{2}}\left\|\eta_6(\boldsymbol{E}_{\mathcal{T}_{k+1}})\right\|_{0;e_*}\lesssim h_{\tau_*}^{\frac{1}{2}}\left\|\eta_6(\boldsymbol{E}_{\mathcal{T}_k})\right\|_{0;e_*}+\eta_{\mathcal{T}_{k+1}}(G,\tau_*)\left\|i\sigma_r^\Sigma\left(\boldsymbol{E}_{\mathcal{T}_k,t}-\boldsymbol{E}_{\mathcal{T}_{k+1},t}\right)\right\|_{0;e_*}.
\end{aligned}$$

Squaring both sides of the above inequalities, using Young's inequality $2ab\leq\alpha a^2+\alpha^{-1}b^2$, summing every elements τ_* and interior edges e_* and using the monotonicity of local mesh sizes and the shape regularity of the mesh $\mathcal{T}$, we obtain the result:

$$\eta^2\left(\boldsymbol{E}_{\mathcal{T}_{k+1}},\mathcal{T}_{k+1}\right)\leq(1+\alpha)\eta^2\left(\boldsymbol{E}_{\mathcal{T}_k},\mathcal{T}_{k+1}\right)+C_\alpha\left\|\boldsymbol{E}_{\mathcal{T}_{k+1}}-\boldsymbol{E}_{\mathcal{T}_k}\right\|^2_{\mathbf{X}(\Omega)}.$$

Proof completed. □

4.2 Estimate between $\boldsymbol{E}_{\mathcal{T}_k}$ and $\boldsymbol{E}_{\mathcal{T}_{k+1}}$

In this section we mainly prove a result about the estimate between $\boldsymbol{E}_{\mathcal{T}_k}$ and $\boldsymbol{E}_{\mathcal{T}_{k+1}}$. In order to prove this theorem, we first need to introduce some conventions and some lemmas to help us prove it.

First, for convenience, we define two new bilinear form $B(\cdot,\cdot)$ and $a(\cdot,\cdot)$ as following:

$$B(E,\varphi)=-(k^2+1)\left(\varepsilon_r E,\varphi\right)_{0;\Omega},$$

where

$$a(E,\varphi)=\bar{a}(E,\varphi)-B(E,\varphi)=\left(\mu_r^{-1}\nabla\times E,\nabla\times\varphi\right)_{0;\Omega}+(\varepsilon_r E,\varphi)_{0;\Omega}+i\left(\sigma_r^{\Sigma}E_t,\varphi_t\right)_{0;\Omega}.$$

Then we define two spaces:

$$\mathcal{D}(\mathcal{T}_k):=\left\{m\in H_0^1(\Omega):m|_\tau\in\mathcal{P}_1,\ \forall\tau\in\mathcal{T}\text{ and }m=\text{ const on }\Sigma\right\},$$

where $\mathcal{P}_1$ denotes the linear polynomial space

$$\mathcal{S}^0(\mathcal{T}_k):=\left\{u_{\mathcal{T}}\in\mathcal{S}(\mathcal{T}_k):(u_{\mathcal{T}},\nabla m_{\mathcal{T}_k})=0,\ \forall m_{\mathcal{T}_k}\in\mathcal{D}(\mathcal{T}_k)\right\}.$$

Now we will introduce several important lemmas that play a crucial role in our proof.

Lemma 4.2 ([10, Lemma 5.53]). *Assume $p\in H^{\zeta}(\text{curl};\Omega)$ with the constant $\frac{1}{2}<\zeta\leq 1$, then we have*

$$\|p-\Pi_{\mathcal{T}}p\|_{\mathbf{X}(\Omega)}\leq Ch_{\mathcal{T}}^{\zeta-\frac{1}{2}}\|p\|_{H^{\zeta}(\text{curl};\Omega).}$$

Lemma 4.3 ([10, Lemma 7.6]). *For every $s_{\mathcal{T}}\in\mathcal{S}^0(\mathcal{T})$, there exists a function $s\in H_0(curl;\Omega)$ satisfying*

$$\nabla\times s=\nabla\times s_{\mathcal{T}},\quad \nabla\cdot s=0,$$

and

$$\|s-s_{\mathcal{T}}\|_{0;\Omega}\lesssim h_{\mathcal{T}}^{\zeta}\|\nabla\times s_{\mathcal{T}}\|_{0;\Omega}$$

with a constant $\zeta\in\left(\frac{1}{2},1\right]$ relying only on region Ω. In particular, when the region Ω is a convex region or a smooth region, $\zeta=1$.

Combining the above lemma, we can prove a more important lemma, which plays a crucial role in proving the theorem.

Lemma 4.4. *Assume $\boldsymbol{E}\in\mathbf{X}(\Omega)$ be the solution of variational problem* (2.1) *and the solution ϑ of dual problem of* (2.1) *satisfies that $\vartheta\in H^{\zeta}(\text{curl};\Omega)$, $\vartheta\in(\frac{1}{2},1]$. For the mesh $\mathcal{T}_k$, $\mathcal{T}_{k+1}$, let $\boldsymbol{E}_{\mathcal{T}_k}\in\mathcal{S}(\mathcal{T}_k)$ and $\boldsymbol{E}_{\mathcal{T}_{k+1}}\in\mathcal{S}(\mathcal{T}_{k+1})$ be the discrete finite element solutions of variational problem* (2.3). *Then for any $c_0>0$, there exists an $h(c_0)$ relying on the domain Ω, wave number k, bounded properties of ε_r, μ_r^{-1} and c_0, such that, if $h_{\mathcal{T}}\leq h(c_0)$, then we have*

$$|B\left(\boldsymbol{E}-\boldsymbol{E}_{\mathcal{T}_{k+1}},\boldsymbol{E}_{\mathcal{T}_{k+1}}-\boldsymbol{E}_{\mathcal{T}_k}\right)|\leq c_0\left\|\boldsymbol{E}-\boldsymbol{E}_{\mathcal{T}_{k+1}}\right\|_{\mathbf{X}(\Omega)}\left\|\boldsymbol{E}_{\mathcal{T}_{k+1}}-\boldsymbol{E}_{\mathcal{T}_k}\right\|_{\mathbf{X}(\Omega).}$$

Proof. By Helmholtz decomposition we can get

$$\boldsymbol{E}_{\mathcal{T}_{k+1}}-\boldsymbol{E}_{\mathcal{T}_k}=\boldsymbol{f}_{\mathcal{T}_{k+1}}+\nabla g_{\mathcal{T}_{k+1}},\tag{4.1}$$

where $\boldsymbol{f}_{\mathcal{T}_{k+1}}\in\mathcal{S}^0(\mathcal{T}_{k+1})$ and $g_{\mathcal{T}_{k+1}}\in\mathcal{D}(\mathcal{T}_{k+1})$. So $\nabla g_{\mathcal{T}_{k+1}}\in\mathcal{S}(\mathcal{T}_{k+1})$. Take curl of (4.1) we have

$$\nabla\times\boldsymbol{f}_{\mathcal{T}_{k+1}}=\nabla\times\left(\boldsymbol{E}_{\mathcal{T}_{k+1}}-\boldsymbol{E}_{\mathcal{T}_k}\right).\tag{4.2}$$

Because of the Galerkin orthogonality we can get $\bar{a}\left(\boldsymbol{E}-\boldsymbol{E}_{\mathcal{T}_{k+1}},\nabla g_{\mathcal{T}_{k+1}}\right)=0$, then we obtain

$$-\left(k^2\varepsilon_r\left(\boldsymbol{E}-\boldsymbol{E}_{\mathcal{T}_{k+1}}\right),\nabla g_{\mathcal{T}_{k+1}}\right)_{0;\Omega}+i\left(\sigma_r^{\Sigma}\left(\boldsymbol{E}-\boldsymbol{E}_{\mathcal{T}_{k+1}}\right)_t,\left(\nabla g_{\mathcal{T}_{k+1}}\right)_t\right)_{0;\Sigma}=0.$$

From [11, Proposition 3.1.21] we have $(\nabla g_{\mathcal{T}_{k+1}})_t=0$ on Σ. It means

$$\left|B\left(\boldsymbol{E}-\boldsymbol{E}_{\mathcal{T}_{k+1}},\nabla g_{\mathcal{T}_{k+1}}\right)\right|=0.$$

So

$$\begin{aligned}&\left|B\left(\boldsymbol{E}-\boldsymbol{E}_{\mathcal{T}_{k+1}},\boldsymbol{E}_{\mathcal{T}_{k+1}}-\boldsymbol{E}_{\mathcal{T}_k}\right)\right|=\left|B(\boldsymbol{E}-\boldsymbol{E}_{\mathcal{T}_{k+1}},\boldsymbol{f}_{\mathcal{T}_{k+1}})\right|\\&\leq C\left\|\boldsymbol{E}-\boldsymbol{E}_{\mathcal{T}_{k+1}}\right\|_{0;\Omega}\left\|\boldsymbol{f}_{\mathcal{T}_{k+1}}\right\|_{0;\Omega}\leq C\left\|\boldsymbol{E}-\boldsymbol{E}_{\mathcal{T}_{k+1}}\right\|_{\mathbf{X}(\Omega)}\left\|\boldsymbol{f}_{\mathcal{T}_{k+1}}\right\|_{0;\Omega}.\end{aligned}$$

Applying Lemma 4.3, we know that there exists $\boldsymbol{f}\in H_0(\mathrm{curl};\Omega)$ such that

$$\nabla\times\boldsymbol{f}=\nabla\times\boldsymbol{f}_{\mathcal{T}_{k+1}},\quad \nabla\cdot\boldsymbol{f}=0,$$

and

$$\left\|\boldsymbol{f}-\boldsymbol{f}_{\mathcal{T}_{k+1}}\right\|_{0;\Omega}\leq Ch_{\mathcal{T}_{k+1}}^{\zeta}\left\|\nabla\times\boldsymbol{f}_{\mathcal{T}_{k+1}}\right\|_{0;\Omega}.\tag{4.3}$$

Combine (4.2) and (4.3) we have

$$\left\|\boldsymbol{f}-\boldsymbol{f}_{\mathcal{T}_{k+1}}\right\|_{0;\Omega}\leq Ch_{\mathcal{T}_{k+1}}^{\zeta}\left\|\nabla\times\left(\boldsymbol{E}_{\mathcal{T}_{k+1}}-\boldsymbol{E}_{\mathcal{T}_k}\right)\right\|_{0;\Omega}.\tag{4.4}$$

Now we have converted the estimate of $\boldsymbol{f}_{\mathcal{T}_{k+1}}$ into an estimate of $\boldsymbol{f}$ by

$$\left\|\boldsymbol{f}_{\mathcal{T}_{k+1}}\right\|_{0;\Omega}\leq\left\|\boldsymbol{f}-\boldsymbol{f}_{\mathcal{T}_{k+1}}\right\|_{0;\Omega}+\|\boldsymbol{f}\|_{0;\Omega}.$$

From (4.4) we already get the estimate of $\|\boldsymbol{f}-\boldsymbol{f}_{\mathcal{T}_{k+1}}\|_{0;\Omega}$. At this point we also hope to get an estimate of $\|\boldsymbol{f}\|_{0;\Omega}$.

By the assumption we know that $\vartheta\in H^{\zeta}(\mathrm{curl};\Omega)$, $\vartheta\in(\frac{1}{2},1]$. Then we have $\vartheta\in\mathbf{X}(\Omega)$. So $\vartheta\in\mathbf{X}(\Omega)$ be the solution corresponding to the following variational problem

$$\bar{a}(q,\vartheta)=(\boldsymbol{f},q)\quad\text{ for all }\quad q\in\mathbf{X}(\Omega).$$

We know $\nabla\cdot\boldsymbol{f}=0$ from Lemma 4.3, and letting $q=\nabla m$ with $m\in H_0^1(\Omega)$ we obtain

$$-\left(k^2\varepsilon_r\nabla m,\vartheta\right)_{0;\Omega}+i\left(\sigma_r^{\Sigma}(\nabla m)_t,\vartheta_t\right)_{0;\Sigma}=0.\tag{4.5}$$

Further, we assume the following regularity result : for a given constant $\zeta\in\left(\frac{1}{2},1\right]$, we have

$$\|\vartheta\|_{H^{\zeta}(\mathrm{curl};\Omega)}\leq C\|\boldsymbol{f}\|_{0;\Omega}.$$

By (4.2) and Lemma 4.3, we have

$$\nabla\times\left(\boldsymbol{f}-\left(\boldsymbol{E}_{\mathcal{T}_{k+1}}-\boldsymbol{E}_{\mathcal{T}_k}\right)\right)=0.$$

Because of Theorem 3.3.9 of [11], we have a $g\in H_0^1(\Omega)$, such that

$$\boldsymbol{f}-\left(\boldsymbol{E}_{\mathcal{T}_{k+1}}-\boldsymbol{E}_{\mathcal{T}_k}\right)=\nabla g.$$

Then by (4.5) we have

$$\bar{a}\left(\boldsymbol{f}-\left(\boldsymbol{E}_{\mathcal{T}_{k+1}}-\boldsymbol{E}_{\mathcal{T}_k}\right),\vartheta\right)=\bar{a}(\nabla g,\vartheta)=0.$$

From the proof of Lemma 4.3 we can get that f not only belongs to $H_0(\mathrm{curl};\Omega)$, but also to $H^s(\Omega)$, where $s>\frac{1}{2}$. By Theorem 3.9 of [10], we know $f|_\Sigma\in H^{s-1/2}(\Omega)\subset L^2(\Omega)$. So $f\in\mathbf{X}(\Omega)$. Now let $q=\boldsymbol{f}$ in dual problem, we have

$$\begin{aligned}
&\|\boldsymbol{f}\|_{0;\Omega}^2=\bar{a}(\boldsymbol{f},\vartheta)\\
=&\bar{a}\left(\boldsymbol{f}-\left(\boldsymbol{E}_{\mathcal{T}_{k+1}}-\boldsymbol{E}_{\mathcal{T}_k}\right),\vartheta\right)+\bar{a}\left(\boldsymbol{E}_{\mathcal{T}_{k+1}}-\boldsymbol{E}_{\mathcal{T}_k},\vartheta\right)\\
=&\bar{a}\left(\boldsymbol{E}_{\mathcal{T}_{k+1}}-\boldsymbol{E}_{\mathcal{T}_k},\vartheta\right)\\
=&\bar{a}\left(\boldsymbol{E}_{\mathcal{T}_{k+1}}-\boldsymbol{E}_{\mathcal{T}_k},\vartheta-\Pi_{\mathcal{T}}\vartheta\right)\\
\le&C\left\|\boldsymbol{E}_{\mathcal{T}_{k+1}}-\boldsymbol{E}_{\mathcal{T}_k}\right\|_{\mathbf{X}(\Omega)}\|\vartheta-\Pi_{\mathcal{T}}\vartheta\|_{\mathbf{X}(\Omega)}\\
\le&C\left\|\boldsymbol{E}_{\mathcal{T}_{k+1}}-\boldsymbol{E}_{\mathcal{T}_k}\right\|_{\mathbf{X}(\Omega)}h_{\mathcal{T}}^{\zeta-\frac{1}{2}}\|\vartheta\|_{H^\zeta(\mathrm{curl};\Omega)}\\
\le&Ch_{\mathcal{T}}^{\zeta-\frac{1}{2}}\left\|\boldsymbol{E}_{\mathcal{T}_{k+1}}-\boldsymbol{E}_{\mathcal{T}_k}\right\|_{\mathbf{X}(\Omega)}\|\boldsymbol{f}\|_{0;\Omega}.
\end{aligned}$$

Therfore, we have

$$\|\boldsymbol{f}\|_{0;\Omega}\le Ch_{\mathcal{T}}^{\zeta-\frac{1}{2}}\left\|\boldsymbol{E}_{\mathcal{T}_{k+1}}-\boldsymbol{E}_{\mathcal{T}_k}\right\|_{\mathbf{X}(\Omega)}.$$

Applying the above result and noting that $h_{\mathcal{T}_{k+1}}\le h_{\mathcal{T}_k}$, we obtain

$$\begin{aligned}
\left\|\boldsymbol{f}_{\mathcal{T}_{k+1}}\right\|_{0;\Omega}=&\left\|\boldsymbol{f}_{\mathcal{T}_{k+1}}-\boldsymbol{f}+\boldsymbol{f}\right\|_{0;\Omega}\\
\le&\left\|\boldsymbol{f}_{\mathcal{T}_{k+1}}-\boldsymbol{f}\right\|_{0;\Omega}+\|\boldsymbol{f}\|_{0;\Omega}\\
\le&Ch_{\mathcal{T}_{k+1}}^{\zeta}\left\|\nabla\times\left(\boldsymbol{E}_{\mathcal{T}_{k+1}}-\boldsymbol{E}_{\mathcal{T}_k}\right)\right\|_{0;\Omega}+Ch_{\mathcal{T}_k}^{\zeta-\frac{1}{2}}\left\|\boldsymbol{E}_{\mathcal{T}_{k+1}}-\boldsymbol{E}_{\mathcal{T}_k}\right\|_{E;\Omega}\\
\le&C_0h_{\mathcal{T}_k}^{\zeta-\frac{1}{2}}\left\|\boldsymbol{E}_{\mathcal{T}_{k+1}}-\boldsymbol{E}_{\mathcal{T}_k}\right\|_{\mathbf{X}(\Omega)}.
\end{aligned}$$

Combine the above result we have

$$B\left(\boldsymbol{E}-\boldsymbol{E}_{\mathcal{T}_{k+1}},\boldsymbol{E}_{\mathcal{T}_{k+1}}-\boldsymbol{E}_{\mathcal{T}_k}\right)\le C_0h_{\mathcal{T}_k}^{\zeta-\frac{1}{2}}\left\|\boldsymbol{E}-\boldsymbol{E}_{\mathcal{T}_{k+1}}\right\|_{\mathbf{X}(\Omega)}\left\|\boldsymbol{E}_{\mathcal{T}_{k+1}}-\boldsymbol{E}_{\mathcal{T}_k}\right\|_{\mathbf{X}(\Omega)}.$$

Choosing $h(c_0)$ sufficiently small such that $Ch(c_0)^{\zeta-\frac{1}{2}}\le c_0$, then for every $h_{\mathcal{T}_k}<h(c_0)$, we get the result what we want. □

Now that all the preparatory work has been completed, we can give the following theorem and its proof.

Theorem 4.1. *Assume $\boldsymbol{E}\in\mathbf{X}(\Omega)$ be the solution of variational problem. For the mesh $\mathcal{T}_k$, $\mathcal{T}_{k+1}$, let $\boldsymbol{E}_{\mathcal{T}_k}\in\mathcal{S}(\mathcal{T}_k)$ and $\boldsymbol{E}_{\mathcal{T}_{k+1}}\in\mathcal{S}(\mathcal{T}_{k+1})$ be the discrete finite element solutions of variational problem. Then for any $0<c_0<1$, there exists a constant $h(c_0)$ relying on the parameter k, the region Ω, c_0 and bounded properties of μ_r^{-1}, ε_r and σ_r^{Σ}, satisfying, if $h_{\mathcal{T}}\le h(c_0)$, then we have*

$$\left\|\boldsymbol{E}-\boldsymbol{E}_{\mathcal{T}_{k+1}}\right\|_{\mathbf{X}(\Omega)}^2\le\frac{1}{1-c_0}\left\|\boldsymbol{E}-\boldsymbol{E}_{\mathcal{T}_k}\right\|_{\mathbf{X}(\Omega)}^2-\left\|\boldsymbol{E}_{\mathcal{T}_{k+1}}-\boldsymbol{E}_{\mathcal{T}_k}\right\|_{\mathbf{X}(\Omega)}^2. \tag{4.6}$$

Proof. We notice that $\left(\sigma_r^{\Sigma}(\boldsymbol{E}-\boldsymbol{E}_{\mathcal{T}_k})_t,(\boldsymbol{E}-\boldsymbol{E}_{\mathcal{T}_k})_t\right)_{0;\Omega}$, $\left(\varepsilon_r(\boldsymbol{E}-\boldsymbol{E}_{\mathcal{T}_k}),(\boldsymbol{E}-\boldsymbol{E}_{\mathcal{T}_k})\right)_{0;\Omega}$ and $\left(\mu_r^{-1}\nabla\times(\boldsymbol{E}-\boldsymbol{E}_{\mathcal{T}_k}),\nabla\times(\boldsymbol{E}-\boldsymbol{E}_{\mathcal{T}_k})\right)_{0;\Omega}$ are all real number. So

$$\begin{aligned}\left\|\boldsymbol{E}-\boldsymbol{E}_{\mathcal{T}_k}\right\|_{\mathbf{X}(\Omega)}^2=&\mathrm{Re}\left\{a(\boldsymbol{E}-\boldsymbol{E}_{\mathcal{T}_k},\boldsymbol{E}-\boldsymbol{E}_{\mathcal{T}_k})\right\}+\mathrm{Im}\left\{a(\boldsymbol{E}-\boldsymbol{E}_{\mathcal{T}_k},\boldsymbol{E}-\boldsymbol{E}_{\mathcal{T}_k})\right\}.\\ =&\mathrm{Re}\left\{a\left(\boldsymbol{E}-\boldsymbol{E}_{\mathcal{T}_{k+1}}+\boldsymbol{E}_{\mathcal{T}_{k+1}}-\boldsymbol{E}_{\mathcal{T}_k},\boldsymbol{E}-\boldsymbol{E}_{\mathcal{T}_{k+1}}+\boldsymbol{E}_{\mathcal{T}_{k+1}}-\boldsymbol{E}_{\mathcal{T}_k}\right)\right\}\\ &+\mathrm{Im}\left\{a\left(\boldsymbol{E}-\boldsymbol{E}_{\mathcal{T}_{k+1}}+\boldsymbol{E}_{\mathcal{T}_{k+1}}-\boldsymbol{E}_{\mathcal{T}_k},\boldsymbol{E}-\boldsymbol{E}_{\mathcal{T}_{k+1}}+\boldsymbol{E}_{\mathcal{T}_{k+1}}-\boldsymbol{E}_{\mathcal{T}_k}\right)\right\}.\end{aligned}$$

Because $a\left(\boldsymbol{E}-\boldsymbol{E}_{\mathcal{T}_{k+1}},\boldsymbol{E}_{\mathcal{T}_{k+1}}-\boldsymbol{E}_{\mathcal{T}_k}\right)+a\left(\boldsymbol{E}_{\mathcal{T}_{k+1}}-\boldsymbol{E}_{\mathcal{T}_k},\boldsymbol{E}-\boldsymbol{E}_{\mathcal{T}_{k+1}}\right)\in\mathbb{R}$, so we can get

$$\begin{aligned}\left\|\boldsymbol{E}-\boldsymbol{E}_{\mathcal{T}_k}\right\|_{\mathbf{X}(\Omega)}^2=&\mathrm{Re}\left\{a\left(\boldsymbol{E}-\boldsymbol{E}_{\mathcal{T}_{k+1}},\boldsymbol{E}-\boldsymbol{E}_{\mathcal{T}_{k+1}}\right)\right\}+\mathrm{Im}\left\{a\left(\boldsymbol{E}-\boldsymbol{E}_{\mathcal{T}_{k+1}},\boldsymbol{E}-\boldsymbol{E}_{\mathcal{T}_{k+1}}\right)\right\}\\ &+\mathrm{Re}\left\{a\left(\boldsymbol{E}_{\mathcal{T}_{k+1}}-\boldsymbol{E}_{\mathcal{T}_k},\boldsymbol{E}_{\mathcal{T}_{k+1}}-\boldsymbol{E}_{\mathcal{T}_k}\right)\right\}+\mathrm{Im}\left\{a\left(\boldsymbol{E}_{\mathcal{T}_{k+1}}-\boldsymbol{E}_{\mathcal{T}_k},\boldsymbol{E}_{\mathcal{T}_{k+1}}-\boldsymbol{E}_{\mathcal{T}_k}\right)\right\}\\ &+2\mathrm{Re}\left\{a\left(\boldsymbol{E}-\boldsymbol{E}_{\mathcal{T}_{k+1}},\boldsymbol{E}_{\mathcal{T}_{k+1}}-\boldsymbol{E}_{\mathcal{T}_k}\right)\right\}\\ =&\left\|\boldsymbol{E}-\boldsymbol{E}_{\mathcal{T}_{k+1}}\right\|_{\mathbf{X}(\Omega)}^2+\left\|\boldsymbol{E}_{\mathcal{T}_{k+1}}-\boldsymbol{E}_{\mathcal{T}_k}\right\|_{\mathbf{X}(\Omega)}^2+2\mathrm{Re}\left\{a\left(\boldsymbol{E}-\boldsymbol{E}_{\mathcal{T}_{k+1}},\boldsymbol{E}_{\mathcal{T}_{k+1}}-\boldsymbol{E}_{\mathcal{T}_k}\right)\right\}\\ =&\left\|\boldsymbol{E}-\boldsymbol{E}_{\mathcal{T}_{k+1}}\right\|_{\mathbf{X}(\Omega)}^2+\left\|\boldsymbol{E}_{\mathcal{T}_{k+1}}-\boldsymbol{E}_{\mathcal{T}_k}\right\|_{\mathbf{X}(\Omega)}^2\\ &+2\mathrm{Re}\left\{\overline{a}\left(\boldsymbol{E}-\boldsymbol{E}_{\mathcal{T}_{k+1}},\boldsymbol{E}_{\mathcal{T}_{k+1}}-\boldsymbol{E}_{\mathcal{T}_k}\right)-B\left(\boldsymbol{E}-\boldsymbol{E}_{\mathcal{T}_{k+1}},\boldsymbol{E}_{\mathcal{T}_{k+1}}-\boldsymbol{E}_{\mathcal{T}_k}\right)\right\}.\end{aligned}$$

Because of the Galerkin orthogonality we obtain $\overline{a}\left(\boldsymbol{E}-\boldsymbol{E}_{\mathcal{T}_{k+1}},\boldsymbol{E}_{\mathcal{T}_{k+1}}-\boldsymbol{E}_{\mathcal{T}_k}\right)=0$, so

$$\left\|\boldsymbol{E}-\boldsymbol{E}_{\mathcal{T}_k}\right\|_{\mathbf{X}(\Omega)}^2=\left\|\boldsymbol{E}-\boldsymbol{E}_{\mathcal{T}_{k+1}}\right\|_{\mathbf{X}(\Omega)}^2+\left\|\boldsymbol{E}_{\mathcal{T}_{k+1}}-\boldsymbol{E}_{\mathcal{T}_k}\right\|_{\mathbf{X}(\Omega)}^2-2\mathrm{Re}\left\{B\left(\boldsymbol{E}-\boldsymbol{E}_{\mathcal{T}_{k+1}},\boldsymbol{E}_{\mathcal{T}_{k+1}}-\boldsymbol{E}_{\mathcal{T}_k}\right)\right\}.$$

Then we have

$$\begin{aligned}\left\|\boldsymbol{E}-\boldsymbol{E}_{\mathcal{T}_{k+1}}\right\|_{\mathbf{X}(\Omega)}^2=&\left\|\boldsymbol{E}-\boldsymbol{E}_{\mathcal{T}_k}\right\|_{\mathbf{X}(\Omega)}^2-\left\|\boldsymbol{E}_{\mathcal{T}_{k+1}}-\boldsymbol{E}_{\mathcal{T}_k}\right\|_{\mathbf{X}(\Omega)}^2+2\mathrm{Re}\left\{B\left(\boldsymbol{E}-\boldsymbol{E}_{\mathcal{T}_{k+1}},\boldsymbol{E}_{\mathcal{T}_{k+1}}-\boldsymbol{E}_{\mathcal{T}_k}\right)\right\}\\ \le&\left\|\boldsymbol{E}-\boldsymbol{E}_{\mathcal{T}_k}\right\|_{\mathbf{X}(\Omega)}^2-\left\|\boldsymbol{E}_{\mathcal{T}_{k+1}}-\boldsymbol{E}_{\mathcal{T}_k}\right\|_{\mathbf{X}(\Omega)}^2+2\left|B\left(\boldsymbol{E}-\boldsymbol{E}_{\mathcal{T}_{k+1}},\boldsymbol{E}_{\mathcal{T}_{k+1}}-\boldsymbol{E}_{\mathcal{T}_k}\right)\right|\\ \le&\left\|\boldsymbol{E}-\boldsymbol{E}_{\mathcal{T}_k}\right\|_{\mathbf{X}(\Omega)}^2-\left\|\boldsymbol{E}_{\mathcal{T}_{k+1}}-\boldsymbol{E}_{\mathcal{T}_k}\right\|_{\mathbf{X}(\Omega)}^2+2c_0\left\|\boldsymbol{E}-\boldsymbol{E}_{\mathcal{T}_{k+1}}\right\|_{\mathbf{X}(\Omega)}\left\|\boldsymbol{E}_{\mathcal{T}_{k+1}}-\boldsymbol{E}_{\mathcal{T}_k}\right\|_{\mathbf{X}(\Omega)},\end{aligned}$$

by applying AM-GM Inequality we can obtain the result. □

4.3 Convergence of the AEFEM

At this point we need an additional lemma to prove the convergence of AEFEM. The lemma is explained as follows:

Lemma 4.5 ([8, Lemma 7]). *Assume a marking parameter $\sigma\in(0,1)$, given a $\mathcal{T}_{k+1}$ be a conforming and shape regular triangulation which is refined from a conforming and shape regular triangulation $\mathcal{T}_k$ applying the Dörfler marking strategy. And have a $\boldsymbol{E}_{\mathcal{T}_k}\in\mathcal{S}(\mathcal{T}_k)$ be the finite element discrete solution of variational problem* (2.3). *Then there have a constant $\gamma\in(0,1)$ relying on σ, satisfying*

$$\eta^2(\boldsymbol{E}_{\mathcal{T}_k},\mathcal{T}_{k+1})\leq\gamma\eta^2(\boldsymbol{E}_{\mathcal{T}_k},\mathcal{T}_k). \tag{4.7}$$

Combine Lemmas 4.1 and 4.5, we could get the following result.

Theorem 4.2. *There have a parameter $\xi\in(0,1)$ relying only on the parameter σ applied in the marking strategy, satisfying*

$$\eta^2\left(\boldsymbol{E}_{\mathcal{T}_{k+1}},\mathcal{T}_{k+1}\right)\leq\xi\eta^2\left(\boldsymbol{E}_{\mathcal{T}_k},\mathcal{T}_k\right)+C_\xi\left\|\boldsymbol{E}_{\mathcal{T}_{k+1}}-\boldsymbol{E}_{\mathcal{T}_k}\right\|^2_{\mathbf{X}(\Omega)},$$

where the constant C_ξ depends only on ξ, k, bounded properties of ε, μ_r^{-1}, σ_r^{Σ} and the shape regularity of the mesh.

With all the preparations in the previous sections, the proof of convergence of AEFEM is given below.

Theorem 4.3. *Let $\boldsymbol{E}\in\mathbf{X}(\Omega)$ be the solution of variational problem* (2.1). *Assuming that the initial mesh size h_0 is sufficiently small and the marking parameter $\sigma\in(0,1)$. Then have constants $0<\gamma_1<1$ and $0<\gamma_2<1$, relying only on σ, k and the shape regularity of $\mathcal{T}_0$, satisfying*

$$\left\|\boldsymbol{E}-\boldsymbol{E}_{\mathcal{T}_{k+1}}\right\|^2_{\mathbf{X}(\Omega)}+\gamma_1\eta^2\left(\boldsymbol{E}_{\mathcal{T}_{k+1}},\mathcal{T}_{k+1}\right)\leq\gamma_2\left(\left\|\boldsymbol{E}-\boldsymbol{E}_{\mathcal{T}_k}\right\|^2_{\mathbf{X}(\Omega)}+\gamma_1\eta^2(\boldsymbol{E}_{\mathcal{T}_k},\mathcal{T}_k)\right).$$

Proof. The proof of the theorem is contained in [8]. For completeness we sketch the proof here. We give a constant ξ in Theorem 4.2, without loss of generality we assume $\gamma_1=C_\xi^{-1}\in(0,1)$. By adding $\gamma_1\eta^2\left(\boldsymbol{E}_{\mathcal{T}_{k+1}},\mathcal{T}_{k+1}\right)$ to both sides of (4.6), then add $\gamma_2\left\|\boldsymbol{E}-\boldsymbol{E}_{\mathcal{T}_k}\right\|^2_{\mathbf{X}(\Omega)}$ to the right of the inequality and subtract $\gamma_2\left\|\boldsymbol{E}-\boldsymbol{E}_{\mathcal{T}_{k+1}}\right\|^2_{\mathbf{X}(\Omega)}$, where $\gamma_2\in(0,1)$ is a specific constant, using Theorem 4.2 to eliminate $\left\|\boldsymbol{E}_{\mathcal{T}_{k+1}}-\boldsymbol{E}_{\mathcal{T}_k}\right\|^2_{\mathbf{X}(\Omega)}$ we have

$$\begin{aligned}
&\left\|\boldsymbol{E}-\boldsymbol{E}_{\mathcal{T}_{k+1}}\right\|^2_{\mathbf{X}(\Omega)}+\gamma_1\eta^2\left(\boldsymbol{E}_{\mathcal{T}_{k+1}},\mathcal{T}_{k+1}\right)\\
\leq&\frac{1}{1-c_0}\left\|\boldsymbol{E}-\boldsymbol{E}_{\mathcal{T}_k}\right\|^2_{\mathbf{X}(\Omega)}-\left\|\boldsymbol{E}_{\mathcal{T}_{k+1}}-\boldsymbol{E}_{\mathcal{T}_k}\right\|^2_{\mathbf{X}(\Omega)}+\gamma_1\eta^2\left(\boldsymbol{E}_{\mathcal{T}_{k+1}},\mathcal{T}_{k+1}\right)\\
\leq&\frac{1}{1-c_0}\left\|\boldsymbol{E}-\boldsymbol{E}_{\mathcal{T}_k}\right\|^2_{\mathbf{X}(\Omega)}-\left\|\boldsymbol{E}_{\mathcal{T}_{k+1}}-\boldsymbol{E}_{\mathcal{T}_k}\right\|^2_{\mathbf{X}(\Omega)}+\gamma_1\left(\xi\eta^2\left(\boldsymbol{E}_{\mathcal{T}_k},\mathcal{T}_k\right)+C_\xi\left\|\boldsymbol{E}_{\mathcal{T}_{k+1}}-\boldsymbol{E}_{\mathcal{T}_k}\right\|^2_{\mathbf{X}(\Omega)}\right)
\end{aligned}$$

$$
\begin{aligned}
&=\frac{1}{1-c_0}\left\|\boldsymbol{E}-\boldsymbol{E}_{\mathcal{T}_k}\right\|^2_{\mathbf{X}(\Omega)}+\gamma_1\xi\eta^2(\boldsymbol{E}_{\mathcal{T}_k},\mathcal{T}_k)\\
&=\gamma_2\left\|\boldsymbol{E}-\boldsymbol{E}_{\mathcal{T}_k}\right\|^2_{\mathbf{X}(\Omega)}+\left(\frac{1}{1-c_0}-\gamma_2\right)\left\|\boldsymbol{E}-\boldsymbol{E}_{\mathcal{T}_k}\right\|^2_{\mathbf{X}(\Omega)}+\gamma_1\xi\eta^2(\boldsymbol{E}_{\mathcal{T}_k},\mathcal{T}_k)\\
&\leq\gamma_2\left(\left\|\boldsymbol{E}-\boldsymbol{E}_{\mathcal{T}_k}\right\|^2_{\mathbf{X}(\Omega)}+\frac{\left[(1-c_0)^{-1}-\gamma_2\right]C_1+\gamma_1\xi}{\gamma_2}\eta^2(\boldsymbol{E}_{\mathcal{T}_k},\mathcal{T}_k)\right).
\end{aligned}
$$

In the above proof, we also used the upper bound to $\left\|\boldsymbol{E}-\boldsymbol{E}_{\mathcal{T}_k}\right\|^2_{\mathbf{X}(\Omega)}$. Therefore, we can choose γ_2 to satisfy the following formula

$$\gamma_1=\frac{\left[(1-c_0)^{-1}-\gamma_2\right]C_1+\gamma_1\xi}{\gamma_2}.$$

That is

$$\gamma_2=\frac{(1-c_0)^{-1}C_1+\gamma_1\xi}{C_1+\gamma_1}.$$

It is known from Lemma 4.4 that when h_0 is sufficiently small, a constant c_0 satisfying the following formula can be obtained:

$$c_0<1-\left(1+C_1^{-1}\gamma_1(1-\xi)\right)^{-1}.$$

We know $\gamma_2<1$ by the above equalities. By the above inequalities, there exist constants $\gamma_2\in(0,1)$ and $\gamma_1\in(0,1)$, we have

$$\left\|\boldsymbol{E}-\boldsymbol{E}_{\mathcal{T}_{k+1}}\right\|^2_{\mathbf{X}(\Omega)}+\gamma_1\eta^2\left(\boldsymbol{E}_{\mathcal{T}_{k+1}},\mathcal{T}_{k+1}\right)\leq\gamma_2\left(\left\|\boldsymbol{E}-\boldsymbol{E}_{\mathcal{T}_k}\right\|^2_{\mathbf{X}(\Omega)}+\gamma_1\eta^2(\boldsymbol{E}_{\mathcal{T}_k},\mathcal{T}_k)\right).$$

Proof completed. □

5 Numerical results

In this section, we provide several numerical examples that aim to validate our analysis and showcase the efficacy of our residual-based posteriori error indicator for the model problems (1.1). For the sake of simplicity, h represents the mesh size. Throughout all the examples, we set the value of wave number k to 1.

We have provided a total of three calculation examples. Example 5.1 demonstrates a scenario where the solution is relatively smooth and presents a comparison between uniform refinements and adaptive refinements. Example 5.2 showcases a situation with local singularities in the solution and provides a comparison between uniform refinements and adaptive refinements. Example 5.3 illustrates the phenomenon of graphene surface plasmons. In the accompanying image, we can clearly observe this phenomenon along with the local refinement results of the mesh.

Example 5.1. We give the domain of Maxwell equation as $[-1,1]^2$, and let the parameters $\mu_r^{-1}=1$, $\varepsilon_r=-1$ and $\sigma_r^{\Sigma}=0$. We construct the analytical solution as follows

$$\boldsymbol{E}=\begin{pmatrix}\cos(\pi x)\sin(\pi y)\\ \cos(\pi y)\sin(\pi x)\end{pmatrix}.$$

Through calculation, the right-hand source term corresponding to the analytical solution can be obtained

$$\boldsymbol{F}=\begin{pmatrix}\cos(\pi x)\sin(\pi y)\\ \cos(\pi y)\sin(\pi x)\end{pmatrix}.$$

Through simple calculation we can know $\boldsymbol{n}\times\boldsymbol{E}=0$ on $\partial\Omega$.

In Example 5.1, we employ the adaptive method to solve the problem. The Fig. 1 show the image of analytical solution. The result in Fig. 2 show the mesh after adaptive refinement. The result in Fig. 5 shows comparison of convergence rates of uniform refinement and adaptive refinement.

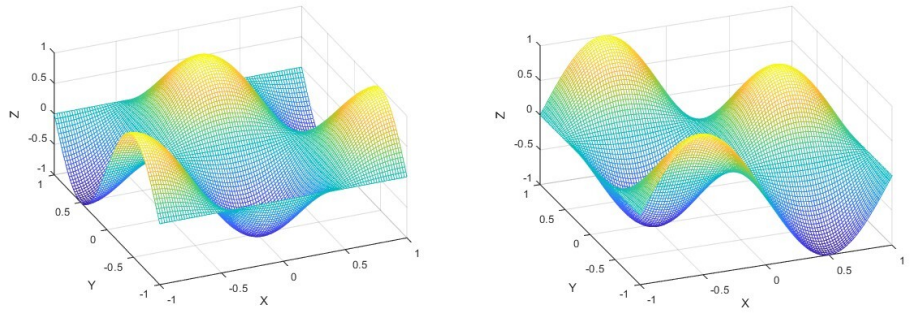

(a) (b)

Figure 1: The image on the left represents the image of the first component of the analytical solution, and the image on the right represents the image of the second component of the analytical solution.

Example 5.2. We give the domain of Maxwell equation as $[-1,1]^2$, and let the parameters $\varepsilon_r=-1$, $\mu_r^{-1}=1$ and $\sigma_r^{\Sigma}=0$. We construct the analytical solution as follows

$$\boldsymbol{E}=\begin{pmatrix}\dfrac{(x^2-1)(y^2-1)}{x^2+y^2+0.01}\\ \dfrac{(x^2-1)(y^2-1)}{x^2+y^2+0.01}\end{pmatrix}.$$

The right-hand source term corresponding to the analytical solution can be obtained by calculation. Through simple calculation we can know $\boldsymbol{n}\times\boldsymbol{E}=0$ on $\partial\Omega$.

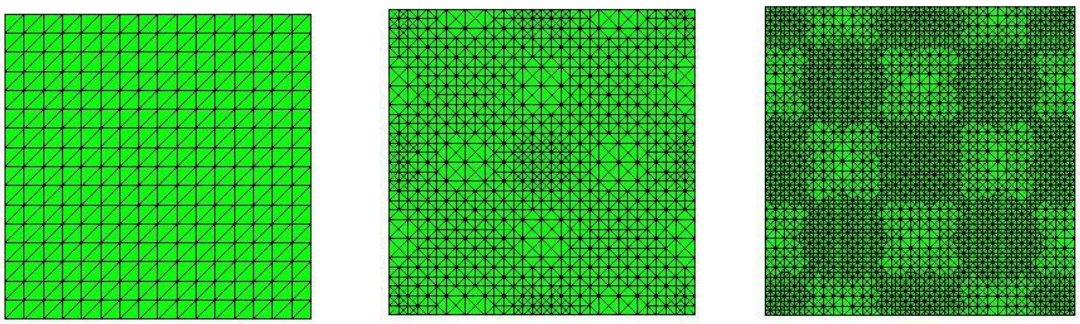

(a) (b) (c)

Figure 2: (a). the initial mesh with 800 DoFs; (b). the adaptive mesh with 4053 DoFs after 7 refinements; (c). the adaptive mesh with 20534 DoFs after 14 refinements.

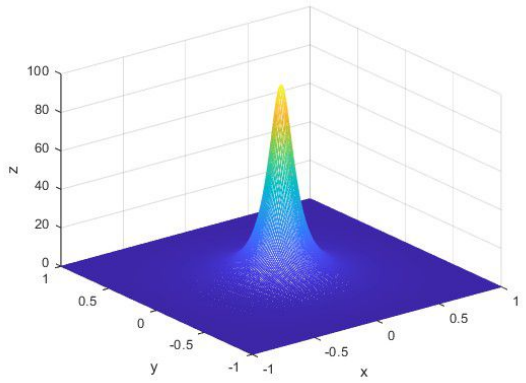

Figure 3: This figure represents the function graph of the first component of the analytical solution in Example 5.2.

In Example 5.2, we employ the adaptive method to solve the problem. The Fig. 3 show the image of analytical solution. The result in Fig. 4 show the mesh after adaptive refinement. The result in Fig. 2 shows comparison of convergence rates of uniform refinement and adaptive refinement.

Example 5.3. We give the domain of Maxwell equation as $[-1,1]^2$ with a graphene layer located at $y=0, -0.99<x<0.99$. Let the parameters $\mu_r^{-1}=1$, $\varepsilon_r=1$. In order to observe the surface plasmon phenomenon, we set the dipole on $(0,0.08)$ and let the graphene surface conductivity $\sigma_r^{\Sigma}=0.001+0.2i$, it means $\boldsymbol{F}=(0,0.08)$.

In Example 5.3, we employ the adaptive method to solve the graphene surface plasmon phenomenon problem. The Fig. 6 shows the initial mesh and physical model. The Fig. 7 shows an adaptively refined mesh image. The Figs. 8 and 9 represents the first component of the real part and imaginary part of the numerical solution. The Fig. 10 rep-

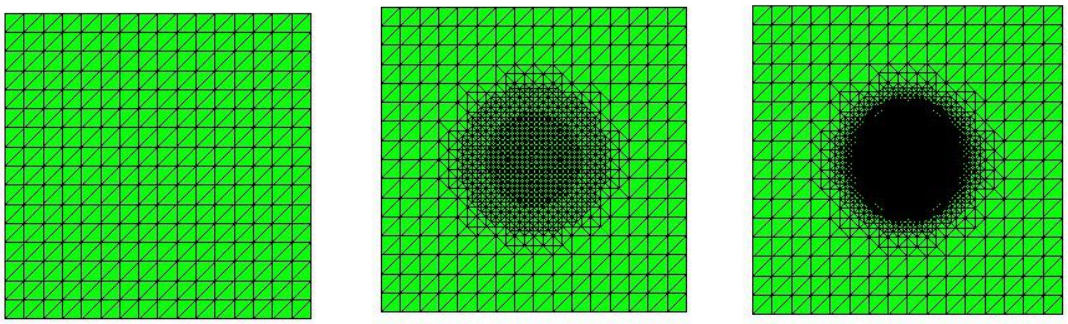

(a) (b) (c)

Figure 4: (a). the initial mesh with 800 DoFs; (b). the adaptive mesh with 3872 DoFs after 9 refinements; (c). the adaptive mesh with 15873 DoFs after 18 refinements.

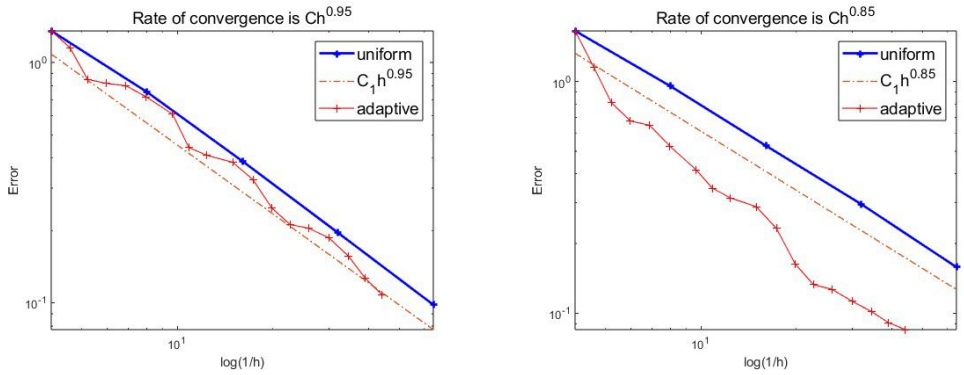

(a) (b)

Figure 5: The blue solid line represents the relationship between error and DoFs in the uniform refinement process, and the red dotted line represents the relationship between error and DoFs in the adaptive refinement process. The red dashed line represents the rate of convergence of uniform refinement. (a). Example 5.1. (b). Example 5.2.

resents the partial enlargement of the plasmon phenomenon on graphene surfaces. The Fig. 11 represents analysis of the errors between our proposed new method and existing methods.

Example 5.4. We give the domain of Maxwell equation as $[-1,1]^2$ with a graphene layer, the physical model is given on the left side of Fig. 6. Let the parameters $\mu_r^{-1}=1$, $\varepsilon_r=1$. In order to observe the surface plasmon phenomenon, we set the dipole on $(0,0.08)$ and let the graphene surface conductivity $\sigma_r^{\Sigma}=0.001+0.2i$, it means $boldsymbolF=(0,0.08)$. The boundary condition is Absorbing Boundary Condition

$$\nu\times\mu_r^{-1}\nabla\times\mathbf{E}=-i\sqrt{\mu_r^{-1}}\varepsilon_r\mathbf{E}_T \quad \text{on} \quad \partial\Omega.$$

In Example 5.4, we first give the numerical results under more complex boundary

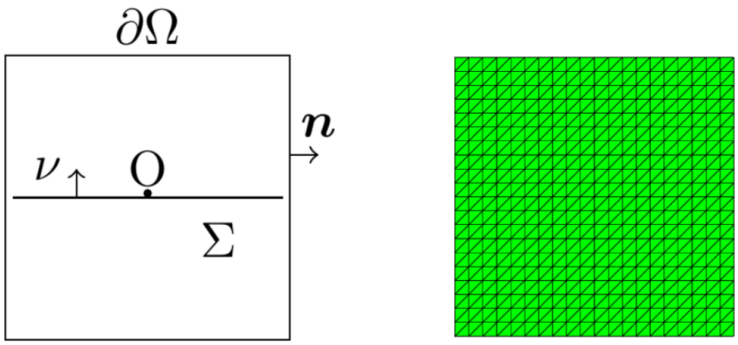

Figure 6: Left: The initial mesh with 1240 degrees of DoFs. Right: A schematic diagram of the physical model. In the diagram, the symbol O represents the source, Σ represents the graphene layer, ν represents the normal vector of the graphene layer Σ, $\partial\Omega$ represents the boundary of the domain, and $\boldsymbol{n}$ represents the normal vector of $\partial\Omega$.

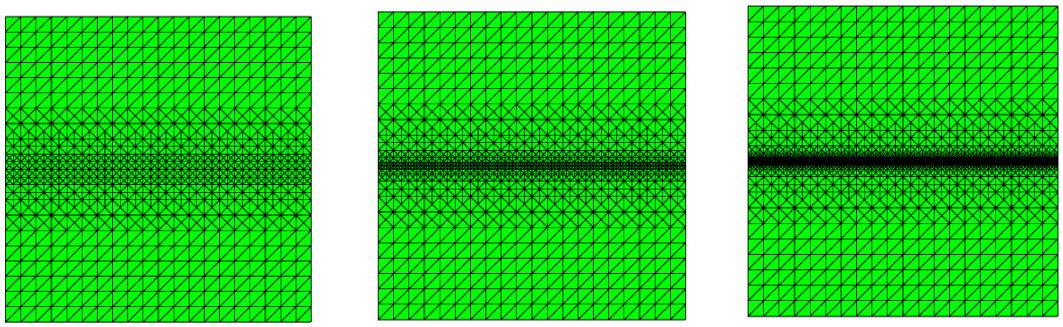

(a) (b) (c)

Figure 7: (a). the adaptive mesh with 2704 DoFs after 5 refinements; (b). the adaptive mesh with 5897 DoFs after 10 refinements; (c). the adaptive mesh with 19453 DoFs after 18 refinements.

conditions (Absorbing Boundary Condition), see Fig. 12.

Then we consider the case of variable coefficients, where we adopt the Perfectly Matched Layer. A perfectly matched layer (PML) is an artificial absorbing layer for wave equations, commonly used to truncate computational regions in numerical methods to simulate problems with open boundaries [29]. We can regard PML as a transformation of the coefficients:

$$\begin{cases} \bar{\mu}_r^{-1} = \dfrac{\mu_r^{-1}}{d}, \\ \bar{\varepsilon}_r = A^{-1}\varepsilon_r B^{-1}, \\ \bar{\sigma}_r^{\Sigma} = C^{-1}\sigma_r^{\Sigma} B^{-1}. \end{cases}$$

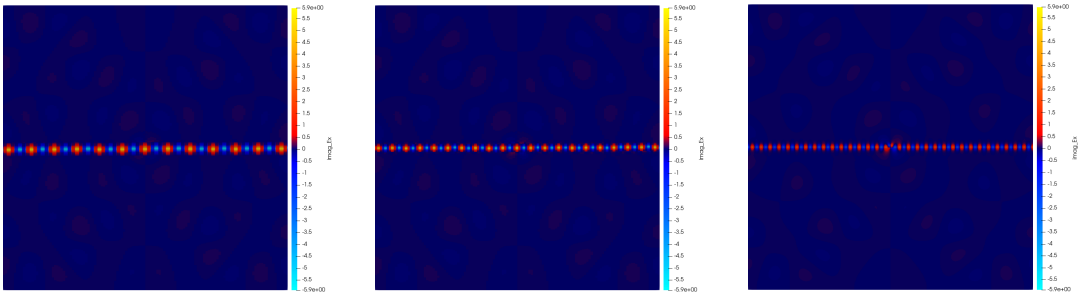

(a) (b) (c)

Figure 8: (a). The first component of the imaginary part of the numerical solution after 5 refinements; (b). The first component of the imaginary part of the numerical solution after 10 refinements; (c). The first component of the imaginary part of the numerical solution after 18 refinements.

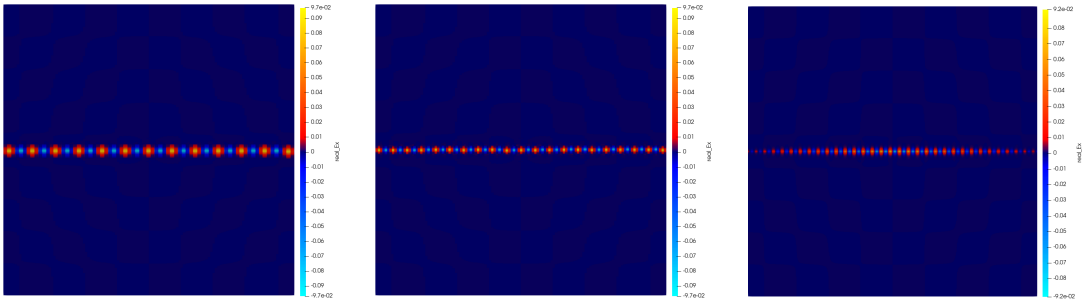

(a) (b) (c)

Figure 9: (a). The first component of the real part of the numerical solution after 5 refinements; (b). The first component of the real part of the numerical solution after 10 refinements; (c). The first component of the real part of the numerical solution after 18 refinements.

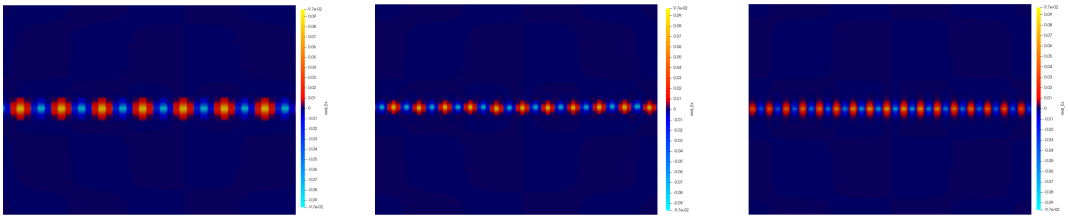

(a) (b) (c)

Figure 10: A partial enlargement of the plasmon phenomenon on graphene surfaces.

Here A, B, and C are all 2×2 matrices:

$$A = T_{e_x e_r}^{-1}\,\mathrm{diag}\left(\frac{1}{\bar{d}^2},\frac{1}{d\bar{d}}\right)T_{e_x e_r},$$

$$B = T_{e_x e_r}^{-1}\,\mathrm{diag}(d,\bar{d})\,T_{e_x e_r},$$

$$C = T_{e_x e_r}^{-1}\,\mathrm{diag}\left(\frac{1}{\bar{d}},\frac{1}{d}\right)T_{e_x e_r},$$

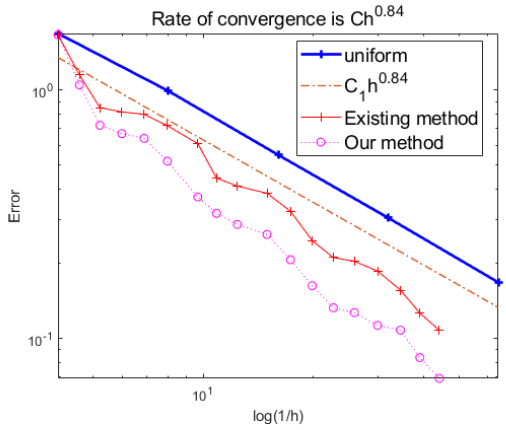

Figure 11: The blue solid line represents the result of uniform refinement, the red solid line represents the error of the existing error estimator, and the pink circle line represents the error of our method.

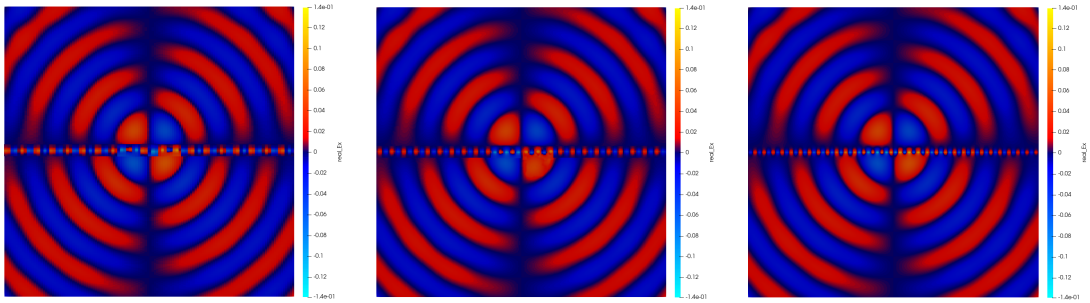

(a) (b) (c)

Figure 12: (Absorbing Boundary Condition) (a). The first component of the real part of the numerical solution after 7 refinements; (b). The first component of the real part of the numerical solution after 14 refinements; (c). The first component of the real part of the numerical solution after 18 refinements.

in which

$$d=1+is(r),$$
$$\bar{d}=1+i\Big/r\int_{\rho}^{r}s(\tau)\mathrm{d}\tau.$$

Here e_r denotes radial direction, e_x denotes x-axis direction, $r=e_r\cdot x$, $s(\tau)$ is an appropriately chosen, nonnegative scaling function and $T_{e_xe_r}$ is the rotation matrix which rotates e_r onto e_x. In Example 5.4, when using PML, we set nonnegative scaling function $s(\tau)=4$ and adopt the above coefficient transformation, and we can get the following numerical results, see Fig. 13.

Next, we consider a case with more complex boundary shape. Here we consider a disk with a hole in the middle. The center of the disk is at $(0,-3)$, the radius of the hole

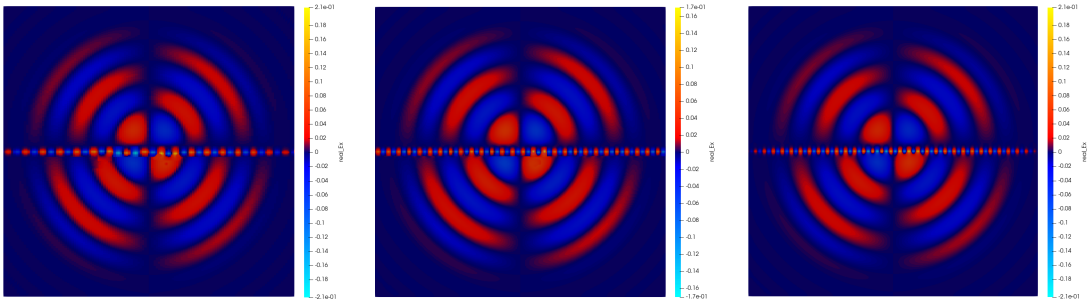

(a) (b) (c)

Figure 13: (Perfectly Matched Layer) (a). The first component of the real part of the numerical solution after 7 refinements; (b). The first component of the real part of the numerical solution after 14 refinements; (c). The first component of the real part of the numerical solution after 18 refinements.

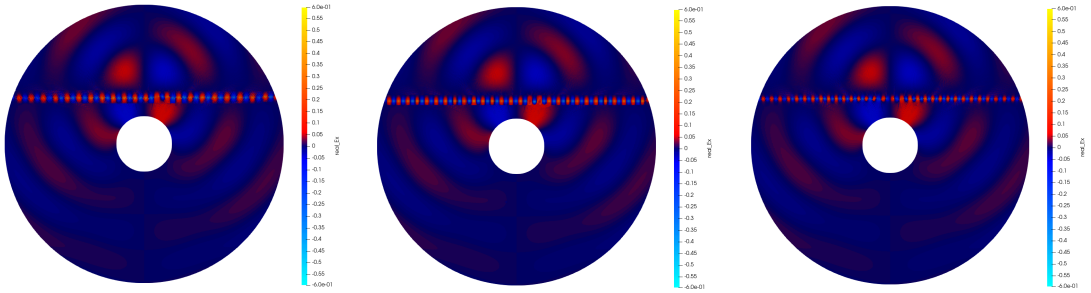

(a) (b) (c)

Figure 14: (Perfectly Matched Layer) (a). The first component of the real part of the numerical solution after 7 refinements; (b). The first component of the real part of the numerical solution after 14 refinements; (c). The first component of the real part of the numerical solution after 18 refinements.

is equal to 1, the radius of the disk is equal to 5, the dipole is placed at $(0,0.08)$, and the graphene layer is located at $y=0$. We can get the following numerical results, see Fig. 14.

6 Conclusions

In this paper, we establish the convergence of the posterior error estimator designed by us and validate our findings through numerical results. The anticipated local refinement is generated in regions where graphene surface polaritons occur, thereby fulfilling the objective of conducting high-precision numerical calculations. At the same time, under some more complex boundary conditions, complex boundary shapes and variable coefficients, we have relatively good numerical results.

Acknowledgements

Yang's research was supported by NSFC Projects (No. 12171411), Hunan Outstanding Youth Fund (No. 2022JJ10043), National Key Research and Development Program of China (No. 2023YFA1009100). Mao's research was supported by Hunan Provincial Innovation Foundation for Postgraduate, China (No. CX20230604), Key Project of Hunan Education Department (No. 23A0143).

References

[1] J. CARDOSO, Electromagnetics through the Finite Element Method: A Simplified Approach using Maxwell's Equations, Crc Press, 2016.
[2] L. LI, AND P. BETTESS, Adaptive Finite Element Methods: A Review, (1997).
[3] P. BERINI, AND I. DE LEON, *Surface plasmon–polariton amplifiers and lasers,* Nature Photonics, 6 (2012), pp. 16–24.
[4] P. MONK, *An analysis of Nédélec's method for the spatial discretization of Maxwell's equations,* J. Comput. Appl. Math., 47 (1993), pp. 101–121.
[5] G. COHEN, AND P. MONK, *Mur-Nédélec finite element schemes for Maxwell's equations,* Comput. Methods Appl. Mech. Eng., 169 (1999), pp. 197–217.
[6] A. ANEES, AND L. ANGERMANN, *Time domain finite element method for Maxwell's equations,* IEEE Access, 7 (2019), pp. 63852–63867.
[7] Z. CHEN, L. WANG, AND W. ZHENG, *An adaptive multilevel method for time-harmonic Maxwell equations with singularities,* SIAM J. Sci. Comput., 29 (2007), pp. 118–138.
[8] B. HE, W. YANG, AND H. WANG, *Convergence analysis of adaptive edge finite element method for variable coefficient time-harmonic Maxwell's equations,* J. Comput. Appl. Math., 376 (2020), 112860.
[9] J. CHÖBERL, *A posteriori error estimates for Maxwell equations,* Math. Comput., 77 (2008), pp. 633–649.
[10] P. MONK, Finite Element Methods for Maxwell's Equations, Oxford University Press, 2003.
[11] F. ASSOUS, P. CIARLET, AND S. LABRUNIE, Mathematical Foundations of Computational Electromagnetism, Springer, 2018.
[12] R. HOLLAND, *Finite-difference solution of Maxwell's equations in generalized nonorthogonal coordinates,* IEEE Trans. Nuclear Sci., 30 (1983), pp. 4589–4591.
[13] P. MONK, *Analysis of a finite element method for Maxwell's equations,* SIAM J. Numer. Anal., 29 (1992), pp. 714–729.
[14] S. BRENNER, J. GEDICKE, AND L. SUNG, *Hodge decomposition for two-dimensional time-harmonic Maxwell's equations: impedance boundary condition,* Math. Methods Appl. Sci., 40 (2017), pp. 370–390.
[15] J. NÉDÉLEC, *Mixed finite elements in* $\mathbb{R}^3$, Numerische Mathematik, 35 (1980), pp. 315–341.
[16] J. ZHANG, L. ZHANG, AND W. XU, *Surface plasmon polaritons: physics and applications,* J. Phys. D: Appl. Phys.. 45 (2012), 113001.
[17] Y. BLUDOV, A. FERREIRA, N. PERES, AND M. VASILEVSKIY, *A primer on surface plasmon-polaritons in graphene,* Int. J. Mod. Phys. B, 27 (2013), 1341001.
[18] J. HAJNAL, *Singularities in the transverse fields of electromagnetic waves. II. Observations on the electric field,* Proceedings of the Royal Society of London. A. Mathematical And Physical Sciences, 414 (1987), pp. 447–468.

[19] G. NEMOVA, AND R. KASHYAP, *Fiber-Bragg-grating-assisted surface plasmon-polariton sensor,* Opt. Lett., 31 (2006), pp. 2118–2120.
[20] A. ZAYATS, I. SMOLYANINOV, AND A. MARADUDIN, *Nano-optics of surface plasmon polaritons,* Phys. Rep., 408 (2005), pp. 131–314.
[21] W. AHN, D. RATCHFORD, P. PEHRSSON, AND B. SIMPKINS, *Surface plasmon polariton-induced hot carrier generation for photocatalysis,* Nanoscale, 9 (2017), pp. 3010–3022.
[22] R. NOCHETTO, K. SIEBERT, AND A. VEESER, *Theory of adaptive finite element methods: an introduction,* Multiscale, Nonlinear and Adaptive Approximation: Dedicated to Wolfgang Dahmen on the Occasion of His 60th Birthday, (2009), pp. 409–542.
[23] W. DÖRFLER, *A convergent adaptive algorithm for Poisson's equation,* SIAM J. Numer. Anal., 33 (1996), pp. 1106–1124.
[24] J. CASCON, C. KREUZER, R. NOCHETTO, AND K. SIEBERT, *Quasi-optimal convergence rate for an adaptive finite element method,* SIAM J. Numer. Anal., 46 (2008), pp. 2524–2550.
[25] C. CARSTENSEN, AND R. HOPPE, Convergence Analysis of an Adaptive Edge Finite Element Method for the 2d Eddy Current Equations, (2005).
[26] R. HOPPE, AND J. SCHÖBERL, *Convergence of adaptive edge element methods for the 3D eddy currents equations,* J. Comput. Math., (2009), pp. 657–676.
[27] P. FORKNER, Finite Difference Time Domain (FTDT) Simulation of Optical Waveguides, (The University of Tulsa, 2016).
[28] M. BUGAJ, AND M. WNUK, *The influence examination of dielectric parameters on bandwidth in multilayer aperture-coupled microstrip antennas with utilization the FDTD method,* MIKON 2008-17th International Conference On Microwaves, Radar And Wireless Communications, (2008), pp. 1–4.
[29] J. BERENGER, *A perfectly matched layer for the absorption of electromagnetic waves,* J. Comput. Phys., 114 (1994), pp. 185–200.